Assessment of integration of methane-reduced ceria chemical looping CO_2/H_2O splitting cycle to an oxy-fired power plant

Azharuddin Farooqui[1,2], Archishman Bose[1], Marta Boaro[3], Jordi Llorca[2], and Massimo Santarelli[1,4]

[1]Department of Energy, Politecnico di Torino, Italy

[2]Institute of Energy Technologies, Department of Chemical Engineering and Barcelona Research Center in Multiscale Science and Engineering, Universitat Politècnica de Catalunya, Barcelona, Spain

[3]Polytechnic Department of Engineering and Architecture (DPIA), Universita di Udine, Italy

[4]Department of Energy Technology, KTH Royal Institute of Technology, Brinellvägen Stockholm, Sweden

Corresponding email id: azharuddin.xxx@polito.it

Abstract:

In this paper, we investigated the effect of reaction kinetics and moving bed reactors for chemical looping (CO_2/H_2O) splitting unit (CL) that produces syngas and fed back to the power plant to gain the efficiency loss due to carbon capture. The reduction reactor (RED) produces methane is partially oxidized to make syngas and reducing the non-stoichiometric ceria which is transported to oxidation reactor (OXI) where the flue gases (CO_2 and H_2O) split to produce syngas. We developed the kinetics for methane reduced ceria and CO_2/H_2O splitting in a tubular reactor for an operating temperature range of (900–1100 °C) for different methane concentration which yielded to Avrami-Erofeev (AE3) model fits well for both redox reaction with different reaction constants. A moving bed reactors system is developed representing RED and OXI reactors of CL unit with kinetics hooked to the model in Aspen Plus with FORTRAN code. The effect of thermodynamics and the kinetics of redox reaction was investigated in the proposed integrated plant. The CL unit efficiency obtained is 42.8% for kinetic-based CL unit compares to 64% for thermodynamic based CL unit. However, the maximum available efficiency of the proposed layout lowered as 50.9% for kinetic-based CL unit plant compare to than 61.5% for thermodynamic based CL unit. However, the proposed plant shows an improvement in the energy efficiency penalty from 11.3% to 3.8% after CCS.

Keywords: Chemical looping, CO_2/H_2O splitting, Kinetics, experimental, system analysis, moving bed reactors.

1. Introduction:

Most sought approach to curb the rise of the carbon dioxide is carbon capture and sequestration (CCS). Mainly two-third of the CO_2 emissions are the result of fossil fuel used power production plants across the globe. CCS is adapted to retrofit the existing heavily invested fossil fuel plants to

work on biomass as fuel or use the conventional carbon capture technologies such as post combustion, pre-combustion or oxy-combustion. Though the CCS technologies maturity for large scale capturing is still yet to demonstrate due to safety and economic feasibility leading to question in investing in viability for large scale sequestration [1]. The mentioned reasons lead to investigate for alternate technologies for CO_2 utilization as a reactant and convert into fuel or hydrocarbons [2–4]. CO_2 splitting for CO production has received much interest after a successful demonstration of water splitting for hydrogen production using a two-step redox cycle with metal oxides as oxygen carriers. [5]. The idea conceived from direct dissociation of water which requires more than 2500^{o}C temperatures. The high temperatures could be attained by solar energy. Later, the operation temperatures for CO_2/H_2O dissociation were proposed by metal oxide which has good oxygen carrying capacity in a two step-redox cycle also termed as solar-thermochemical cycle [6,7]. The metal oxide also called as oxygen carrier take part in two separate reduction and oxidation reaction where solar-thermal reduction of metal oxide loses oxygen and become lower valence metal oxide. In the second step the reduced metal oxide undergoes oxidation reaction with incoming CO_2/H_2O production CO/H_2 [8]. Here, a reduction temperature higher than the oxidation one is the thermodynamic constraint for this process to be attainable, as shown in **Error! Reference source not found.**.

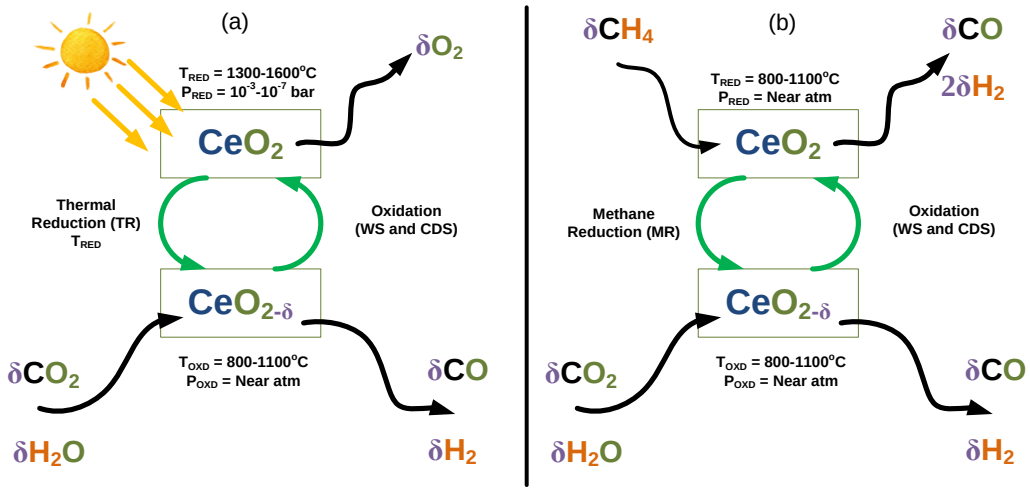

Figure 1: Conceptual scheme of the chemical looping syngas production through (a) solar thermal reduction and (b) methane reduction and corresponding splitting of water and carbon dioxide, usually present in waste gas from industrial applications

Among many investigated metal oxides for CO_2/H_2O dissociation redox reaction, ceria has showed great potential due to its higher oxygen transport capacity, electronic and ionic properties and faster kinetics and it undergoes non-stoichiometric reaction without changing its microstructure at higher temperatures. Following are the thermal reduction and CO_2 dissociation expressed as equation 1 and 2 and also represented in Figure 1a.

$$\text{Thermal reduction: } CeO_2 \rightarrow CeO_{2-\delta} + 0.5\delta O_2(g) \quad (1)$$

$$\text{Oxidation: Oxidation: } CeO_{2-\delta} + \delta CO_2(g) \rightarrow CeO_2 + \delta CO(g) \quad (2)$$

In thermochemical redox cycle, the oxygen release can be achieved either by heating ceria to a high temperature (1600^{o}C) using concentrated solar irradiation (Eq. 1) or by reducing the metal oxide with CH_4, can also termed as reactive-chemical looping redox cycle as equation (3).

Methane reduction: $CeO_2 + \delta CH_4(g) \rightarrow CeO_{2-\delta} + 2\delta H_2O\,(g) + \delta CO_2$ (3)

The challenges associated with solar thermochemical dissociation of CO_2/H_2O to make fuel are related to achieving very high thermal reduction temperatures with the limitation of solar technology. Though this could be attained but the two steps operate at different temperature creating a dynamic temperature swing along with pressure swing would limits the benefits if the process is not designed efficiently. With the fuel reduction step replacing the vacuum operated thermal reduction would eliminate the pressure swing operation making the two-step redox cycle to operate at near atmosphere.

In recent times, the attention to fuel reduction of ceria has increased immensely [9–14]. Some of them were focused with catalyst promoters such as Pt [9] and Rh [15,16] to enhance the reactivity. Structure of the experimental reactor and material form such as powder, reticulated foam, honeycomb, monolithic structure, etc., with promoters and support, also plays role in achieving higher reaction extent [12,17–22]. Nair and Abandes [17] investigated the solar methane reforming and H_2O/CO_2 splitting for ceria and ceria promoted with MgO and Al_2O_3 in a solar thermogravimetric device specially designed for particular experiments. The results reported that for CeO_2 part of the sample is completed converted to Ce_2O_3 after reduction with a remaining in non-stoichiometric form with the global δ <0.5 and reported an activation energy of 109 kJ/mol and a reaction order of 0.62. The maximum δ achieved was 0.37 for pure ceria and with the inert support of MgO, it increased to 0.431. With recent study later in 2017 in Scheffe's group, conducted experiments on solar methane reforming to investigate the performance and extent of reduction along with efficiency with the particle-transport reactor and solar cavity tubular reactor allowing packed bed format for ceria reduction. Both the experiments were testing on different temperature operation with particle reactor being tested 1150-1350^{o}C resulting non-stoichiometry 0.002 to 0.22 [23] while for packed bed setup the 950-1120^{o}C yielded δ from 0.07-0.24 [24]. Otsuka et al [25] studied the reaction mechanism between both doped and undoped ceria for POM, where, the recombination or desorption of the produced H_2 was identified as the rate determining step for the reduction reaction. In a further study, the same author reported activation energy of POM over pure ceria to a value around 160 kJ/mol [26]. Warren et al [27], in a recent work published in 2018 reported the kinetic behaviour related to POM over pure ceria including studying the impact of different factors like the limitation of gas/solid diffusion, gas composition ratio between the reactant and the product, etc. Through experiments conducted at the range between 750^{o}C and 1100^{o}C and atmospheric conditions, and carrying out measurements through a thermogravimetric analyser, activation energy for the reaction was obtained using Arrhenius-type plots [27]. The activation energy reported was much lower, between 20 kJ/mol and 80 kJ/mol, with the higher value being obtained at a δ>0.15. Furthermore, a complete reduction of ceria was reported beyond 900^{o}C [27] though the study do not infer the sample characterization and microstructure analysis to support the claim, as with the ceria phase diagram the structure do not hold if the ceria loses more than 17% of the oxygen from it. Also,

none of the studies, to the best knowledge of the authors have considered model based kinetic approach to report the overall reaction kinetics of POM with ceria reduction. This model specifically benefits in the identification of the rate controlling mechanism, while at the same time assign parameters to the kinetic model, so as to successfully predict the outcomes of the reactions over the entire envelope of the fuel curve [11].

For the oxidation reaction, multiple studies of kinetics of catalytic oxidation of Ce_2O_3 at low temperatures (below 800^oC) with water or CO_2 have been studied and reported in multiple literature, especially due to its applications in catalytic convertors, fuel cells and other applications [11]. Nevertheless, such low temperature studies for catalytic reactions are typically not applicable for higher temperature non-catalytic oxidation reactions. Ishida et al [28] studied the kinetic models for water splitting while Le Gal and Abanades [29] studied and reported the kinetics of both water and CO_2 splitting in the context of solar fuel chemistry. For undoped Ceria, Le Gal et al obtained the second-order power law model to best describe the CDS kinetics, through a surface-limited reaction mechanism, even though no kinetic parameters were reported. "Master Plot" approach [30,31] was used in this regard to analyse the mass gain measured by the thermogravimetric analyser (TGA) during oxidation. Arifin et al [11], uses a modified approach, by separating the experimental effects from material specific H_2 and CO curve rates, reported the WS kinetics to be best described by a first-order kinetic model. All model parameters were also reported, whereby, a low apparent activation energy of 29 kJ/mol was obtained in the range of 750-900^oC. On the other hand, CDS kinetics was found to be surface-mediated phenomena with a much higher complexity than the WS reaction, leading to no one solid state kinetic model (SS) to accurately predict the product yield over the entire range of experimental conditions, 600-875^oC and 10–40 vol% CO_2. This is due to the fact that the SS models, essentially lumped parameter models with a minimal level of detail about the reaction mechanisms, does not account for the transient phenomena occurring during the CDS reactions. Farooqui et al [32] in another recent study, tried to further this limitation for identification of the proper kinetic model for the CDS reaction. The authors compared the different reaction models to experimental data (CO_2 oxidation of reduced ceria in an atmosphere of H_2 at a temperature range of 700-1100^oC) by curve fitting, followed by statistically comparison using the Residual sum of squares (RSS), Akaike information criterion (AICc) and the F-test methods. The Sestak-Berggren (SB) model which is a nested category model of nucleation and grain growth was found to fit best to the experimental data of the CDS reaction together with an activation energy of 79.1 ± 6.5 kJ/mol being obtained [32].

Nevertheless, the different experimental conditions, including experimental artifacts significantly affect the overall outcomes and hence the results of the experiments. A detailed discussion in this regard has been reported by Scheffe et al [33]. This not only results in a wide discrepancy in the reported results, but also in developing a comprehensive model to best describe a reaction over a wide range of temperature and operating conditions. Unlike the model developed by Bulfin et al [34] which comprehensively describes the solar thermal reduction of ceria, over a wide range of operating conditions, not one model exists that can accurately predict the reduction of ceria by methane. In addition, all the oxidation kinetics have been studied after thermal reduction of ceria or H_2 reduction. CO_2 kinetics, being so heavily dependent on the surface phenomena, thus needs to be re-evaluated for oxidizing methane-reduced ceria.

Many studies considering chemical looping CO_2/H_2O splitting were considered thermodynamic equilibrium models to investigate the feasibility of power and fuel such as methanol, dimethyl ether [3,35], jet fuels [36], naphtha [22,36,37], kerosene [37] etc. through industrial processes. These studies projected higher efficiencies as the reduction and oxidation were to occur with chemical equilibrium which does not undergo in heterogeneous thermochemical redox reactions.

Therefore, the kinetics of methane reduction of commercial ceria with subsequent oxidation with CO_2 was investigated with semi-empirical solid state kinetic model development would help in predicting the efficiency of the system. In the following section, a detailed methodology, experimental set-up and results of the kinetics of methane reduction of commercial ceria and oxidation of the reduced methane at isothermal conditions are presented and discussed. Later application of the kinetic model fitted would be used in a moving bed reactor model for reduction and oxidation as a CL unit for an oxi-fired power plant which was studied based on thermodynamic model.

2. Experimental Section

Isothermal redox cycles of CeO_2 commercial powders were performed in a horizontal tubular reactor in the temperature range of 900–1100°C. Methane (CH_4) was used for the ceria reduction to evaluate the reaction kinetics for commercial ceria and explore the maximum non-stoichiometric capacity (δ) achieved at a set-point temperature. Corresponding oxidation with different concentration of carbon dioxide in the oxidation step was performed with the aim to develop the reaction kinetics of reduction and subsequent oxidation of a methane-driven two-step chemical looping cycle with commercial ceria. The temperature swing is thus replaced by isothermal operation for developing the kinetics.

During the reduction, an online mass spectrometer was used to measure the H_2 and CO production during reduction and CO production during the oxidation reaction. Upon analysis of the reactivity data obtained from the experiments, different kinetic models based on alternative reaction mechanisms (i.e., reaction order, geometrical contracting, diffusion, and nucleation models) were compared for the best-fitting model for selection. Hence, the corresponding ceria reduction and oxidation mechanism were identified. The experimental setup comprised a horizontal alumina tubular reactor, a control unit, a gas delivery system and a real-time gas analysis system with an online mass spectrometer as can be seen in Figure 2.

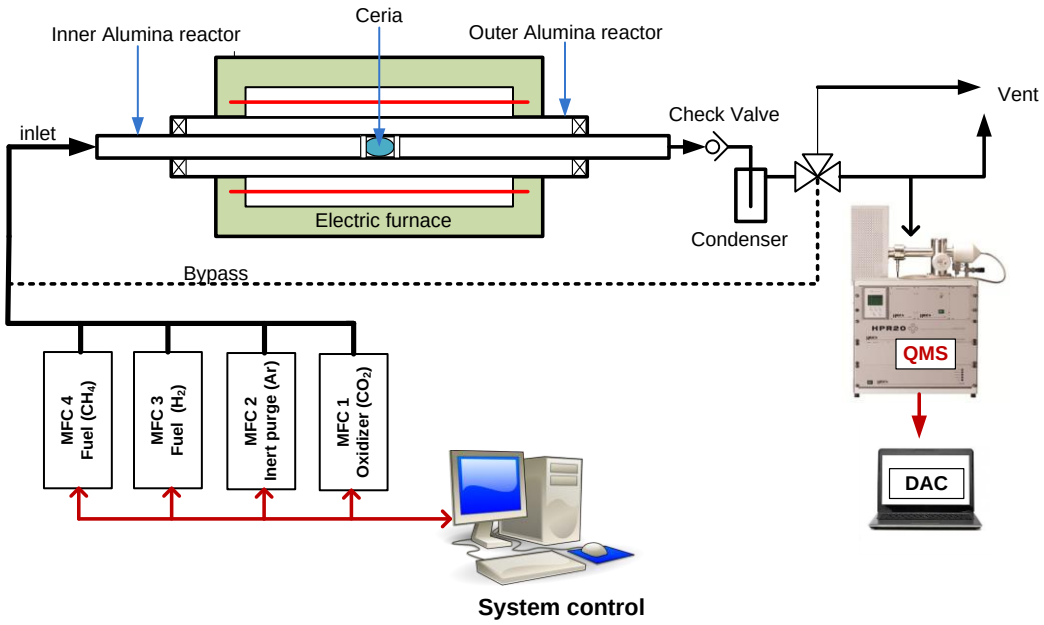

Figure 2. Experimental set-up for testing in micro-reactor configuration

A Quadrupole Mass Spectrometer (QMS) (Hiden Analytical Inc.) was used to analyse the gas composition. Commercial ceria powder from Alfa Aesar (99.95% purity) was chosen for the reaction study. The sample was crushed and sieved to 32µm before the tests. A 250mg amount of ceria powder (m_{CeO_2}) was embedded in alumina wool and placed at the centre of the inner alumina tube. The total flow rate of gases into the reactor during both the reduction and the oxidation steps were maintained constant at 120Nml/min. During both the reduction and the oxidation, the mole fraction of the reactant gases (CH_4 and CO_2 respectively), were varied between 20% and 50%, balance argon. During the reduction, since one mole of methane leads to the formation of 2 moles of H_2 and one mole of CO, the molar flow at the outlet is higher than the inlet. However, as the production of 1 mol of CO leads to the consumption of 1 mol of CO_2, the total molar flow rate throughout the control volume remains constant during the oxidation cycle.

Each experiment was performed in a cycle of four steps. The first step included the ceria reduction step where the mixture of argon and methane was passed over the sample. Different concentrations of CH_4 (20-50%) was passed to evaluate the reduction mechanism. The readings of the QMS were observed to analyse for complete reduction of ceria. However, in the case of lower reaction rates at lower temperatures, the reactant gases were passes for 75 minutes to ensure enough reduction to study the corresponding oxidation. After completion of the reduction cycle, a purging stream of pure Ar was fed for 10 min, to remove the reactants and products present in the fixed bed from the previous cycle. The following step was the oxidation reaction where a mixture of Ar and different concentrations (20-50%) of CO_2 was sent for 15 min. The last step was the purging with pure Argon for approximately 10 min or until the QGA reading was stable enough to begin the next cycle, whichever is earlier. Isothermal redox cycles were performed between the temperature ranges of 900-1100°C. The measure of H_2 and CO concentrations for the reduction cycle and the CO for the

oxidation cycle at the outlet flow of the reactor allowed to extrapolate the reaction rate of the reduction and oxidation reactions respectively. However, for the reduction step, the methane splitting reaction (equation 4) can occur, which would give erroneous results from the reading of the hydrogen measurements due to the formation of H_2 and elementary solid carbon, which would be deposited inside the reactor. Indeed, this would be reflected by the corresponding oxidation, whereby the reaction kinetics would depend not only on the ceria oxidation but also on the Boudard reaction (equation 5).

$$\mathrm{CH_4} \rightarrow \mathrm{C(s)} + 2\mathrm{H_2} \tag{4}$$

$$\mathrm{C(s)} + \mathrm{CO_2} \rightarrow 2\mathrm{CO} \tag{5}$$

Nevertheless, for most parts of the experimental regime, no significant carbon formation was noticed. In any case, the measurements of CO both during the reduction and the oxidation cycle were considered for developing the necessary kinetics as follows:

$$\dot{\omega}_{\mathrm{CO,\ red}} = \frac{X_{CO,out}\dot{n}_{red,out}}{m_{CeO_2}} = \frac{X_{CO,out,red}}{m_{CeO_2}} \frac{P^0 \dot{V}^0_{red,in}}{RT^0} \tag{6}$$

$$\dot{\omega}_{\mathrm{CO,\ oxd}} = \frac{X_{CO,ox-out}\dot{n}_{ox,out}}{m_{CeO_2}} = \frac{X_{CO,ox-out}}{m_{CeO_2}} \frac{P^0 \dot{V}^0_{ox,in}}{RT^0} \tag{7}$$

where $X_{CO,out}$ is the measured mole fraction of CO at the exit of the reactor, $\dot{n}_{out}$ is the total molar outflow rate of the gas mixture for the reduction and oxidation respectively, as per the designation in equations (6) and (7), which are equal to the inlet molar flow, while P^0, T^0 and $\dot{V}^0_{in}$ are the pressure, temperature and the total volumetric inflow rate at standard temperature and pressure (STP) with respect to the two alternate reduction and oxidation cycles. The reaction rates for both the reduction and oxidation cycles have been normalized by the total ceria sample m_{CeO_2} – i.e. 250 mg – used in the measurement. During the entire experiments, a quasi-steady-state was assumed. Hence, the accumulation or depletion effect in the control volume was neglected. This can be attributed to the fact that the residence time of the gases is negligible in relation to the characteristic time of the redox conversion.

The bulk-phase non-stoichiometry change of ceria would be first evaluated through the extrapolated reduction rate, as per the reaction is written in the following equation (Eq. 8). Correspondingly, the bulk-phase non-stoichiometry change of ceria can also be evaluated by extrapolating the oxidation reaction rate based on oxidation with carbon dioxide. The oxidation reaction can be rewritten as per the equation (Eq. 9):

$$\delta_1 \mathrm{CH_4(g)} + \mathrm{CeO_2} \rightarrow \delta_1 \left[\mathrm{CO(g)} + 2\mathrm{H_2(g)}\right] + \mathrm{CeO_{2-\delta_1}} \tag{8}$$

$$CO_2(g) + \frac{1}{\delta} CeO_{2-\delta_1} \rightarrow CO(g) + \frac{1}{\delta} CeO_{2-\delta_2} \quad (9)$$

where the non-stoichiometry reached after the reduction step is represented by δ_1 and δ_2 correspond to the non-stoichiometry at the end of the ceria oxidation step and $\delta=\delta_1-\delta_2$ is the bulk-phase non-stoichiometry change, calculated as per the following equation [32] (Eq. 10):

$$\delta(t) = \frac{n_{oxygen}(t)}{n_{CeO_2}} \quad (10)$$

where $n_{oxygen}(t) = \int_0^t \dot{\omega}_{CO_{red}} dt = \int_0^t \dot{\omega}_{CO_{oxi}} dt$ represents the accumulated release and intake of oxygen ions during the reduction and the oxidation reactions respectively, $n_{CeO_2} = m_{CeO_2} / M_{CeO_2}$ is the moles of ceria used in the experiment, with M_{CeO_2} is its molar mass.

The non-stoichiometry is calculated by the amount of oxygen that the solid can release and accept when reduced by methane and oxidized with CO_2, starting from a neutral state. Therefore, at the end of oxidation, which also represents the completion of one cycle, oxygen vacancies are depleted, and no more oxygen is incorporated in the material. The maximum non-stoichiometry is affected by the temperature, where, an increase in temperature results in an increased rate of oxygen release and hence, an increased availability of vacancies.

3. Material characterization

The lattice structure of the samples were investigated before and after testing the redox cycles for structural integrity using X-ray diffraction (XRD) was performed using a PANalytical X'pert MPD Pro diffractometer with Ni-filtered Cu Kα irradiation (wavelength 1.5406 Å). All samples were scanned in the 2θ range from 5° to 120° with a step size of 0.2°/s. For a rough estimation on sintering effect, the crystallite size of samples before and after the test was calculated from the Scherrer equation (equation 11) based on the reflection with the highest intensity.

$$D = \frac{0.9\lambda}{\beta \cos\theta} \quad (11)$$

D, λ, β, and θ are the grain size, the X-ray wavelength, the width at half maximum intensity, and the Bragg angle respectively. Crystallite micrographs were obtained through a scanning electron microscope (SEM, JSM7800F) at an accelerating voltage of 5 kV.

4. Reactivity results

The results of the tests for methane reduction and the CO_2 splitting performance in terms of the CO production rate (ml/(min-g)) and the total CO yield (ml/g) were investigated. For each point of observation, five consecutive redox cycles are performed to attain stable results. It is observed besides the first cycle, all the other cycles show a consistent repeatability for both the oxidation and the reduction reactions as shown in Figure 3. For the kinetic analysis, the fifth cycle is taken into

consideration. It can also be seen that the H_2/CO ratio for almost 2 for the reported condition but this would increase at a higher temperature accounting for H_2 due to methane splitting. Therefore for developing the kinetic model only CO is considered from both reduction and oxidation step.

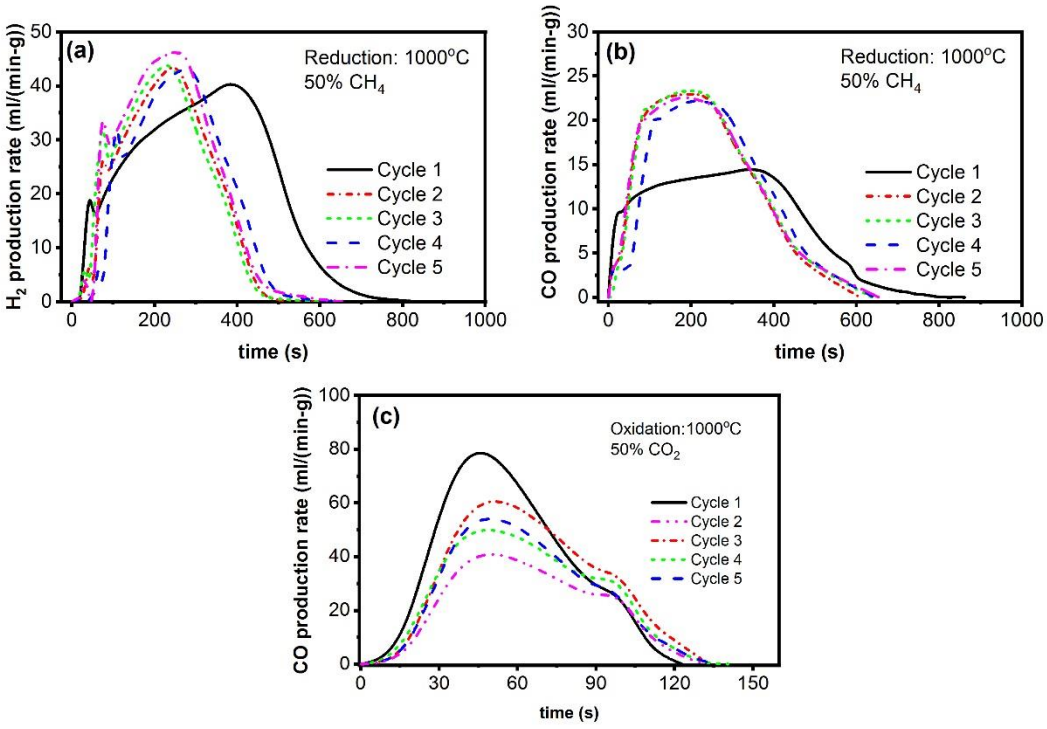

Figure 3 (a) H_2 and (b) CO production rate from the reduction of CeO_2 over 50% CH_4 and (c) oxidation of the reduced metal oxide with 50% CO_2 over five cycles each.

The primary motive behind the set of experiments was to evaluate the performance and the dependence of commercial CeO_2 as oxygen carrier on temperature and reactant gas concentration. Hence a series of tests were performed in different experimental conditions and are described in the following sections.

4.1 Effect of temperature

Figure 4 shows the CO production rate as a function of temperature for both the oxidation and reduction reactions. For both the reactions, the temperature was varied from 900 to 1100^{o}C. In each plot, the reaction rate is characterized by a slow initial stage, a fast-middle stage, also resulting in a peak reaction rate, and subsequently a decrease.

During reduction, the slow increase in the CO release results from the release of oxygen from the crystal lattice of the metal oxide. Both temperature and reactant concentration play a role in determining the maximum rate. Indeed, the relative length of each of the three phases depends much on the reaction temperature, which is especially significant for the reduction reaction. This, in turn, would lead to a much longer time for completion of the reduction with a subsequent lower yield. As can also be seen for both the reduction and oxidation reactions, the peak rate varies non-linearly with

temperature, and for temperatures lower than 900°C, the reaction becomes slow enough to limit the overall non-stoichiometric ceria yield.

For the reduction reaction, the impact of temperature is much more pronounced on the peak product yield, as can be seen from Figure 4(a). From the increase in temperature from 950°C to 1100°C, the peak yield of CO was observed to increase almost six times, with the most marked rise in the yield rate occurring between 1000°C and 1050°C, when the production rate almost triples. Also, with temperature, the peak rate becomes faster and quicker to occur (around 600 secs for 950/1000°C and around 400 secs for 1050°C. At 900°C, no significant peak is even noticed, with a flatter trajectory occurring over a larger time due to the lower amount of available oxygen sites. After the peak yield, the production rate drops rapidly, with a complete reaction taking place in around 1000s for all temperatures beyond 900°C. Thus, a strong temperature dependence of the reduction yield rate profile of methane reduction of ceria, which becomes higher and narrower at a higher temperature.

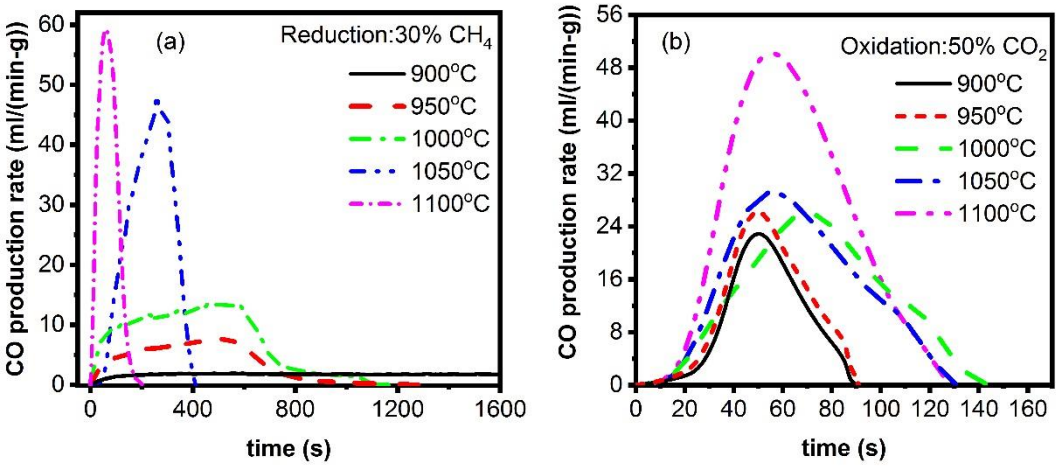

Figure 4 Variation of yield rates of CO in (a) reduction and (b) oxidation of CeO_2 in the redox cycle of methane reduction followed by oxidation with CO_2 with the variation of temperature in the range 900°C and 1100°C; Methane concentration during reduction: 30%; CO_2 concentration during oxidation: 50%, baseline reactor pressure: 1 atm.

On the other hand, for the oxidation reaction, a rapid rise in the CO yield is observed due to the rapid oxygen vacancies ion incorporation. Similar to the reduction reaction, after peak CO yield, the yield drops sharply for all temperatures approaching zero in 80-150 secs. It needs to be mentioned here that the oxidation cycles have experimented directly with the reduction cycles. Therefore, the performance of the oxidation reaction is directly influenced by the net non-stoichiometry generated in the reduction step. In this regard, since a lower non-stoichiometry was generated in the reduction reaction ($\delta = 0.10$) for reduction at 900°C, the net reaction time was lower. However, with an increase in temperature, the peak CO yield becomes higher and wider, indicating a high activation barrier associated with the CO_2 splitting process [38]. Figure 4(b) emphasizes the observed behavior of the peak rates at varying temperature for a fixed CO_2 molar fraction. The strong temperature dependence of CO_2 splitting observed in the present study is evident from the earlier studies as well [39–41].

4.2 Effect of concentration

The effect of the concentration of the reactants on the reduction and the oxidation kinetics of ceria with methane and CO_2 respectively was also investigated. Figure 5 clearly indicates that for both the reduction and the oxidation reaction, the reaction time decreases with an increase in the partial pressure of CH_4 and CO_2 in the feed for reduction and oxidation respectively, together with a higher peak rate of product yield. Similar effects from lower activation energies at higher CH_4 concentration during CH_4 reduction was reported by Warren et al [27] and Zhao et al [42], while for oxidation, Farooqui et al [32] reported similar reaction profiles. An increase in the conversion rate is counter-balanced by a decrease in the conversion time, and hence the net yield remains fairly constant for the point of interest.

For instance, for the reduction at 1000^{o}C, the maximum non-stoichiometry generated at lower concentrations (30% CH_4, balance Argon) was slightly higher, 0.20, than for higher methane concentrations (50% CH_4, balance Argon), around 0.184. On the other hand, the overall net yield of the oxidation with CO_2 remains constant, due to a fixed reduction extent of ceria, the result is completely oxidized ceria.

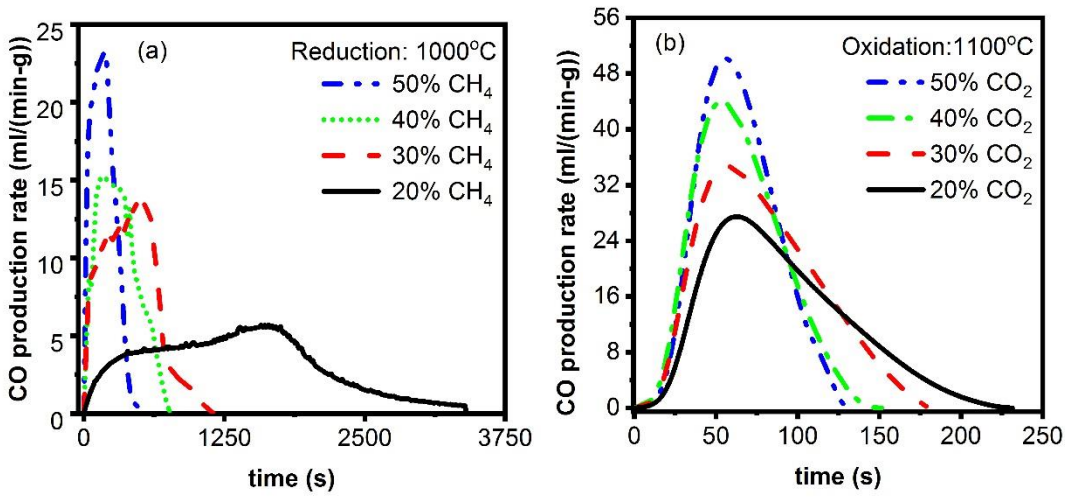

Figure 5 Variation of yield rates of CO in (a) methane reduction of ceria at 1000^{o}C and (b) oxidation of reduced ceria at 1100^{o}C with the variation of concentration of the gaseous reactants at a reactor pressure of 1 atm

Also, as can be seen from Figure 5(a), the peak shifts considerably to a lower time with higher methane concentrations, with a peak yield being noticed at around 200 secs for 50% concentration of methane, while for 20% methane in feed, a peak was obtained only after 1750 sec. In contrary, the oxidation reaction, even though occurring at a higher temperature, does not show such a significant impact of the variation of concentration, as can be noticed from Figure 5(b). The peak remains constant between 60-70 secs range. In relation to the peak rate variation with temperature, the variation was non-linear for the reduction reaction (Figure 5(a)). However, for the oxidation, the peak rate increases linearly with the concentration of CO_2 in the feed. The lower dependence of CO_2 splitting on the concentration of the CO_2 in the feed in comparison to methane for reduction has been reported elsewhere as well [6,32,40,43].

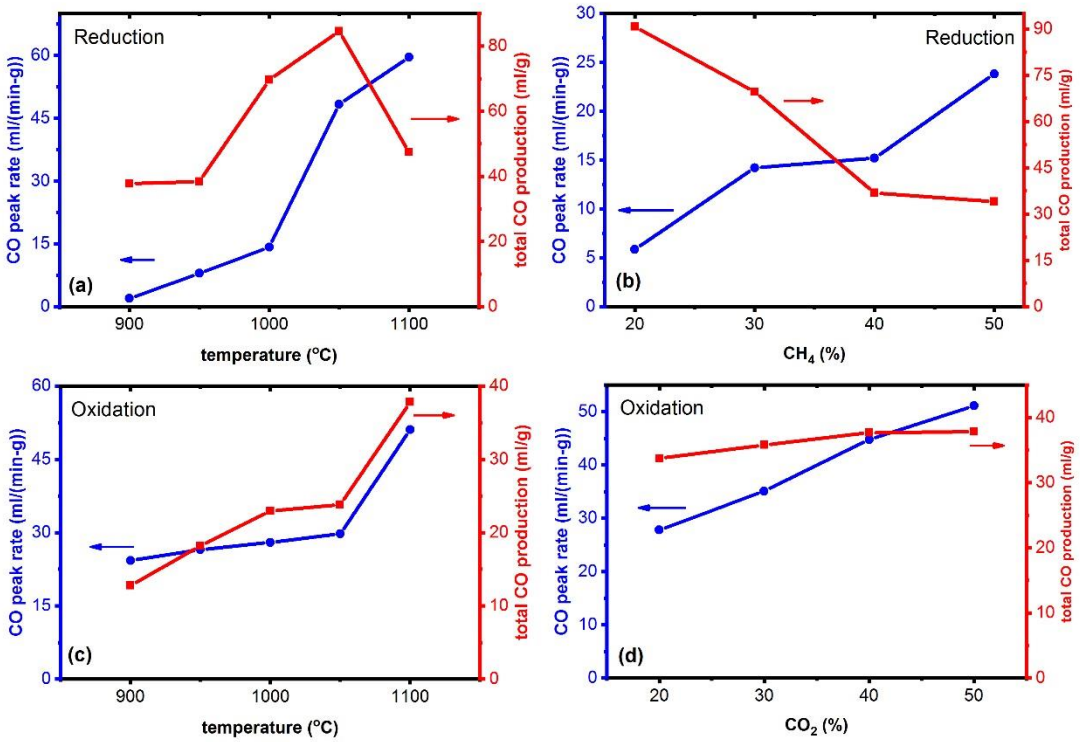

Figure 6 CO peak rate and total CO production for varying temperatures and feed concentrations with CH_4 of 30% and CO_2 of 50% during reduction and oxidation respectively and 1100°C during oxidation.

Figure 6 shows the CO peak production rate and total yield of CO from the reduction of ceria by methane and oxidation by CO_2 for different temperature and concentration of interest. The methane flow was kept constant at 20-50% and the total gas flow was maintained at 120 ml/min for reduction. It is observed from Figure 6(a) the concentration of oxygen vacancies in the ceria increases with increase of temperature from 900-1050°C with total CO production 37.7 – 84.5 ml/g (δ = 0.1-0.23) but at 1100°C drops to 47.9 ml/g (δ=0.12) reason being is that there is evident methane splitting as shown from the microstructural analysis also. Similar non-stoichiometry is reported by Warren et al [24] δ=0.21 at 1035°C. It is worth mentioning that CO peak rates for lower temperature are very low as 2 ml/(min-g) but making the reduction step long for 62 min comparing to 1000°C making to last for 19.5 min with a peak rate of 14.2 ml/(min-g). Therefore, with an increase in temperature the reaction time drops but it is a trade-off to limit the operating temperature to avoid methane splitting. The initial stage of oxidation ends within the 20s but accounts for more than 70% of the overall δ change, while the remaining oxidation leads to a lower change of non-stoichiometry. It is evident that the oxygen-carrying capacity increases due to a higher extent of non-stoichiometry achieved at higher temperatures. Figure 6(b) represents that total CO production decreases from 90.7-34.0 ml/g (δ=0.24-0.17) with an increase of methane concentration from 20-50% at 1000°C, even though the total CO production drops but the CO peak rate increases from 5.8-23.8 ml/(min-g). The decrease of total CO production is due to a decrease in the oxygen vacancies due to carbon deposition at the surface of the sample at a higher concentration of methane, this is also reported by [44].

Figure 6 (c) represents CO peak rate and CO total production increases with an increase in temperature of oxidation. The total CO production rate increases from 12.7-23.8 ml/g (δ=0.1-0.23)

from 900-1050^{o}C and there is a sudden rise in total CO production to 37.8 ml/g for 1100^{o}C. This rise is attributed to reverse boudard reaction of carbon which was formed during reduction leading to the higher rise of CO production. Nonetheless, it is worth mentioning that there is the very little effect is observed of CO_2 concentration during oxidation with 33.7-37.8 ml/g for CO_2 concentration from 20-50% even though the peak rate is increased 27-51 ml/(min-g). It can be noted that the non-stoichiometry increases from 0.07 to 0.21 in the 900–1000°C temperature range for 20% CO_2 mole fraction during oxidation, and a maximum of 0.25 is reached at 1000°C for 30% CO_2 mole fraction. Similar non-stoichiometry results for oxidation are reported in our previous results of H_2 reduction and elsewhere [32,40,43,45].

It is important to mention that methane reduction kinetics is much slower than H_2 reduction and CO production is higher for similar CO_2 concentration during the oxidation step. For instance, in H_2 reduced oxidation step with 20% CO_2 concentration, CO production is 28.5 ml/g compared to 33.7 ml/g when CH_4 is reduced for reduction. Similar results are reported by Zhou [46] for methane reduction for lower temperatures but the oxidation step is replaced by H_2O splitting instead of CO_2.

4.3 Microstructural analysis

XRD patterns of ceria before and after the reaction cycle for different temperatures are analyzed (can be seen Figure S1 in the supplimentary file), revealed a cubic fluorite structure in all the cases of temperature and concentrations. Compared to XRD patterns before cycling, the peaks appear more intense after cycling, which indicates a growth of crystalline grains during the high-temperature process. XRD analysis cannot give information regarding the crystal size (117 nm) because the operating temperature led to a significant growth of crystal size, which resulted higher than 80 nm. In general, for size higher than 80 nm the instrument contribution to the peak width overwhelms the signal from the crystallite size broadening and it is not possible to determine this latter contribution.

SEM characterization helps more to define the splitting processes occurring during the operating conditioning. With 30% CH_4 concentration during reduction at 900°C ceria is present in particles of 60-100 nm that often forms bigger aggregates of 2 microns as shown in Figure 7(a). The size of aggregates of ceria at 1000^{o}C slightly increase with respect to that of the samples treated at 900°C which can be seen in Figure 7(b). At the higher temperature of 1100^{o}C, the carbon is rarely on the sample as observed but instead coated on the rods of SiO_2 which is from quartz wool sheets which are qualitatively approximated to 10-20%. The ceria aggregates resulted in very compact with size varies from 3 microns to 30 microns. But when the methane is fed in higher concentration the carbon deposit is more evident and cover also the ceria aggregates (Figure 7(c)). The amount of carbon revealed on ceria aggregates is not homogeneous, this is due to small carbon sheet deposited also on ceria which in turns drops the CO production rates at higher concentration of methane during reduction. The carbon formed during methane splitting undergoes reverse bourdard reaction forming CO at a higher temperature.

Carbon deposition for methane reduction of ceria at over 1100^{o}C and for a δ of over 0.2 has been reported by Otsuka et al [25,26]. Furthermore, methane cracking has also been reported to be enhanced at temperatures above 1100^{o}C in the presence of alumina (Al_2O_3) [53], which is also the material of the present reactor. In addition, the passing of excess amount of methane or excessive

residence times could also lead to significant carbon deposition, even though not considered as conditions in the present set of experiments [54]. However, Warren et al reported decreased carbon deposition from using platinum crucible as a replacement of alumina or quartz crucible for TGA experimental purpose [27].

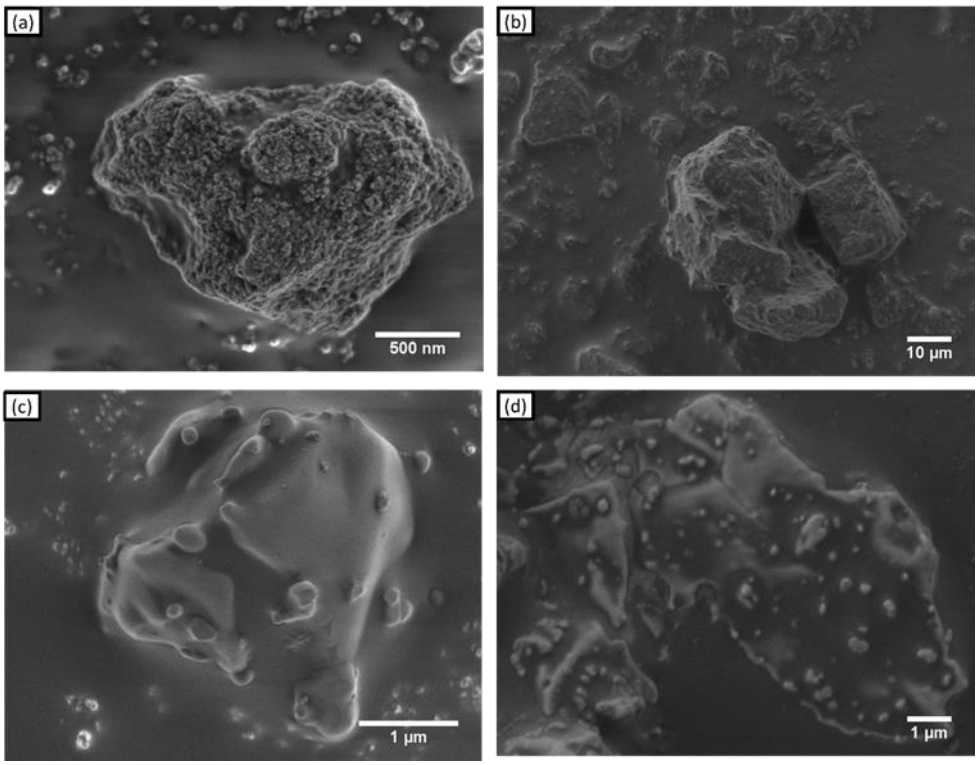

Figure 7 Phases, and compositions in the samples of ceria (a) 900^{o}C (b) 1000^{o}C (c) 1100^{o}C at 30% CH_4 (d) 1000^{o}C at 30% CH_4

5. Kinetic study

The evaluation of kinetic model parameters includes iso-conversion and isothermal reaction analysis [47]. For the present set of reactions, within the working envelope of the chemical looping process for narrow temperature range, the isothermal method was chosen. As reported by Han et al [48] the intra-particle heat gradients can be assumed negligible and thus the particle can be approximated to be isothermal.

In this work, the reaction kinetics study was evaluated by fitting different models to the experimental data to identify the solid-state reaction kinetic mechanistic model for both the reduction and oxidation of ceria. The most common metric adopted for the comparison of reaction models with experimental evidence is the reaction rate, measured in terms of the time profile of reactant conversion or product yield [49]. Three methods were used to compare several solid-state reaction kinetic models presented in supplementary file against isothermal experimental data.

The extent of reaction during the time is an important parameter involved in the kinetic study, which can be derived from the cumulative of the CO produced as equation (12). As CO was chosen

the common parameter for both the reduction and oxidation reactions, hence, the following equation remains valid irrespective of the type of experiment performed.

$$cum\left(\dot{\omega}_{\mathrm{CO,i}}\right) = \sum_{p=1}^{i-1}\left(\dot{\omega}_{\mathrm{CO,p}}\right) + \dot{\omega}_{\mathrm{CO,i}} \tag{12}$$

The extent of reaction (X) for each time instant is given by equation (13).

$$X(t_i) = \frac{cum(\dot{\omega}_{\mathrm{CO,i}})}{cum(\dot{\omega}_{\mathrm{CO,N}})} \tag{13}$$

Alternately, the extent of reaction at time t_i can be defined as the ratio between the i^{th} value of the cumulative and the final value of the cumulative. Essentially, this fixes the X to vary between 0 and 1. This results in the obtaining of the experimental α that could be compared against the X derived from the models.

To obtain the kinetic model, a mathematical equation was being developed and the kinetic expression for the gas-solid reaction was expressed as per the following equation (14) [50]:

$$\frac{dX}{dt} = k_1 \cdot f(X) \cdot [P]^m \tag{14}$$

Where X is the conversion, $k_1 = A\exp\left(-E_a / RT\right)$ and P is the partial pressure of the gas phase reactants (CH_4 or CO_2), m is the reaction order and f(X) is a function of X following the reaction mechanism. The coefficients A and E_a are the Arrhenius parameters; E_a being the activation energy. R is the universal gas constant equal to 8.314 kJ/mol/K.

The first step of calculations involves the fitting of the model to the raw data. This requires Eq. (14) to be transformed to the following equation (15):

$$\frac{dX}{f(X)} = K \cdot dt \tag{15}$$

Where $K = k^1 \cdot P^m$ is expressed in terms of partial pressure of the gas phase reactants. The integral of the reaction model is expressed by integrating equation (16), which can also be expressed in a simplified manner as per equation (17).

$$g(X) = \int_0^{\alpha} \frac{dX}{f(X)} \tag{16}$$

$$g(X) = K \cdot t \tag{17}$$

The slope of the curve g(X) vs t gives the parameter *K*. The slope between natural log of *K* vs 1/T (Eq. 18) provides the activation energy, obtained as a negative slope. The intercept is the value of $\ln(AP^m)$ where P is the partial pressure of the gas phase reactants. The reaction order was thereby

evaluated by plotting ln(AP^m) vs. lnP (Eq. 19) with the slope being the reaction order and the intercept yielding the 'A' value.

$$\ln K = -\frac{E_a}{RT} + \ln A \cdot P^m \tag{18}$$

$$\ln[A \cdot P^m] = \ln A + m \ln P \tag{19}$$

The basic procedure needs to utilize the kinetic expressions of the models reported in table S1 in supplementary file to match the experimental data obtained by evaluating dX/dt vs X and X vs t profiles. This is performed by fitting the value of the K parameter, and hence selecting the models with the smallest residual sum of squares (RSS) and R^2 close to unity.

5.1 Kinetic Parameter Evaluation

Based on the models listed in table S1 in supplementary file, a comprehensive evaluation with all the models was performed, together with finding the least RSS by fitting each model to the experimental results. Nevertheless, Avrami-Erofe'ev (AE3) model was found to fit best with the experimental results for both the reduction and oxidation reactions. The following section summarizes the kinetic results of the two sections of the redox cycle starting from the reduction of ceria with methane.

5.1.1 Ceria reduction by methane

As mentioned, based on the calculation of the least errors of all the models fitted to the experimental results, an average R^2 value of 0.97 was obtained for the AE3 model, showing a good match. After the selection of the kinetic model, the evaluation of the kinetic parameters was carried out.

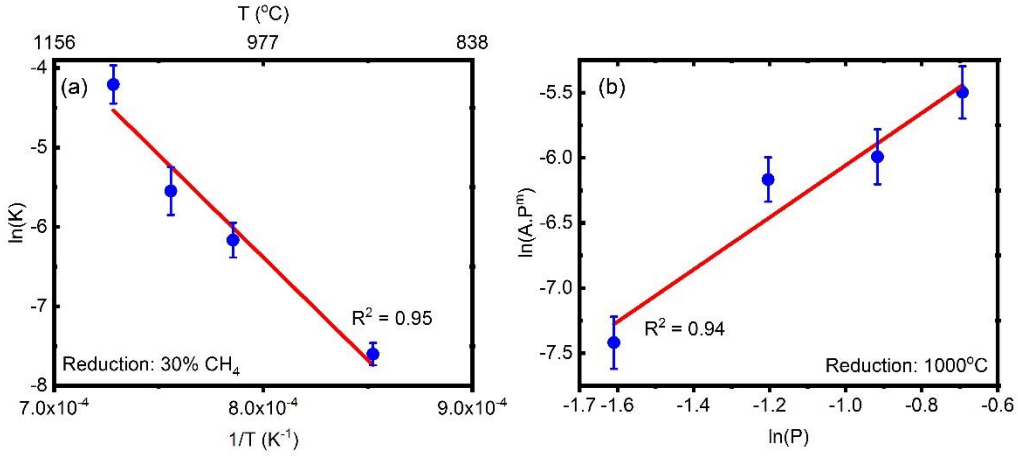

Figure 8 (a) ln(K) vs (1/T) Arrhenius plot of the reduction reaction for AE3 model; (b) ln(AP^m) vs ln(P) plot for reduction reaction order determination.

The ln($A \cdot P^m$), as obtained directly from the slope of the curve g(X) vs t was plotted first versus log of concentration in terms of partial pressure (ln(P)) to obtain the reaction order, as described in

equation (19), as shown in Figure 8(b). The reaction order obtained is 2.0 ± 0.36. Correspondingly, ln(K) was plotted versus the inverse of the temperature (1/T) as described through equation (18). Figure 8 (a) represents the ln(K) vs (1/T) plot reduction of ceria with 30% methane, the average activation energy was calculated as $E_{RED\text{-}CH4}$ = 283.65 ± 0.66 kJ/mol within a 95% confidence level. The pre-exponential factor, $E_{RED\text{-}CH4}$ was calculated as 8.67E9 ± 433 s^{-1}.

Nonetheless, the concentration effect in terms of reactor order was further evaluated through curve fitting and was obtained to vary both with temperature and concentration. In this regard, a regression analysis between m_{RED}, T and P in terms of concentration was carried out for temperatures below 1050°C using statistical methods. The relation obtained is described by the following equation (20) and the corresponding R^2 value obtained was 0.98. Beyond 1050°C, the reaction order was found to remain constant at 2.2.

$$m_{RED} = 19.897 - 0.013 \times [T] - 1.28 \times [P_{CH_4}] \quad (20)$$

Where T is in Kelvin and P is the concentration or partial pressure of the gaseous reactant, considering ideal gas laws.

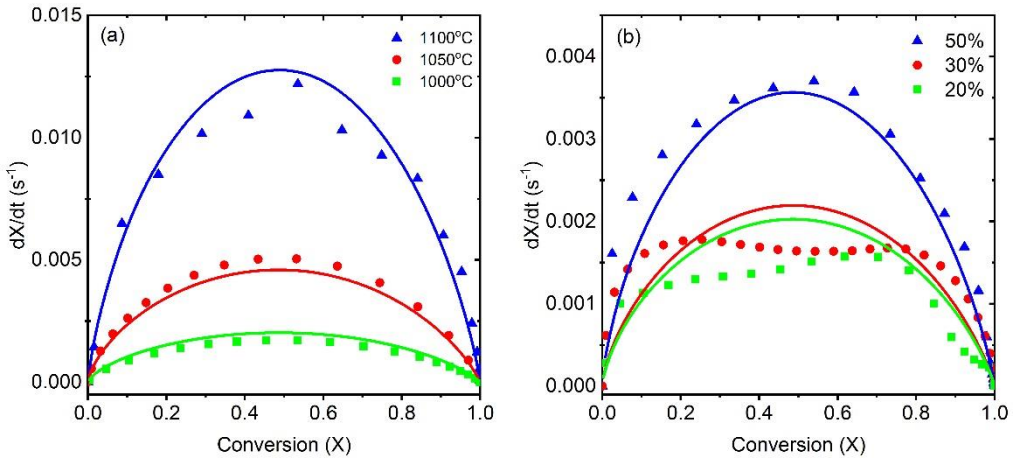

Figure 9 Comparison of the kinetic model and the experimental data for methane reduction of ceria (a) with the variation in temperature, 1000°C, 1050°C, 1100°C and (b) with the concentration of CH_4 of 20%, 30% and 50% for reactor pressure of 1 atm. The symbol represents experimental data and lines represent the kinetic model

The value of activation energy and the other constants obtained in the model fit well to the experimental results, as obtained through curve fitting using the proposed model, shown in the following Figure 9. A good agreement of the results, both with respect to concentration and temperature variation can be seen. It is observed that there is discrete values of activation energies have been reported which varied from 20 kJ/mol to 334.56 kJ/mol [17,27,51] for a variety of conditions of temperature and concentration of the reducer. Warren et al [27] reported that the activation energy varies from 20-80 kJ/mol as the non-stoichiometry (ranging from 0 to 0.35). Otsuka et al [26] reported 160 kJ/mol of activation of methane reduction by ceria with Pt as a catalyst. A similar value of 165-176 kJ/mol is reported by Ramirez Cabrera et al [52] reported the effect of doping of Gd and Nb over ceria. It is reported that the activation energies are reduced by the doping or by using a catalyst with the ceria. The activation energy evaluated in the present

experiments higher than of 221 kJ/mol was reported in the literature [29] but lower than reported 334.56 kJ/mol by Ackermann et al which was evaluated for considering oxygen diffusion in ceria [51]. Even so, no study has reported the complete solid-state kinetic model development for the said reaction. Therefore, no comprehensive comparison with literature data can be done. Nonetheless, a slight over-estimation for lower concentrations are obtained, while for higher concentration, the model slightly underpredicts the yield of the products. Nevertheless, all the results lie within the 95% confidence level and agree well with values obtained in literature, as described earlier.

5.1.2 $CeO_{2-\delta}$ oxidation by CO_2

Like the reduction reaction, a similar curve fitting was performed using least square of errors on all the models listed in Table S1 in supplementary file. As like the reduction reaction, the AE3 model fits best with the experimental results and the average R^2 value obtained was 0.98, showing a good match.

A similar procedure, as discussed for the reduction reaction, to obtain the reaction order and the activation energy was carried out. The $\ln(A \cdot P^m)$, as obtained directly from the slope of the curve g(X) vs t was plotted first versus log of concentration (ln(P)) to obtain the reaction order, as described in equation (19) (Figure 10 (b)). The reaction order obtained is 0.732 ± 0.186. Correspondingly, ln(K), was plotted versus the inverse of temperature (1/T) as described through equation (18). Figure 10(a) represents the ln(K) vs (1/T) plot oxidation with 50% CO_2, the average activation energy was calculated as $E_{0,\ OXI\text{-}CO2}$ 59.68 ± 6.09 kJ/mol. The pre-exponential factor, $A_{0,OXI\text{-}CO2}$ was calculated as 64.48 ± 1.45 s^{-1}.

Nonetheless, the concentration effect in terms of reactor order was further evaluated through curve fitting similarly as before and was obtained to vary both with temperature and concentration. In this regard, a regression analysis between m_{OXI}, T, and P in terms of concentration was carried out for all temperatures and concentrations using statistical methods. The relation obtained is described by the following equation (21) and the corresponding R^2 value obtained was 0.985.

$$m_{OXI} = 0.002 \times [T] - 7.5 \times [P_{CO_2}] - 1.996 \quad (21)$$

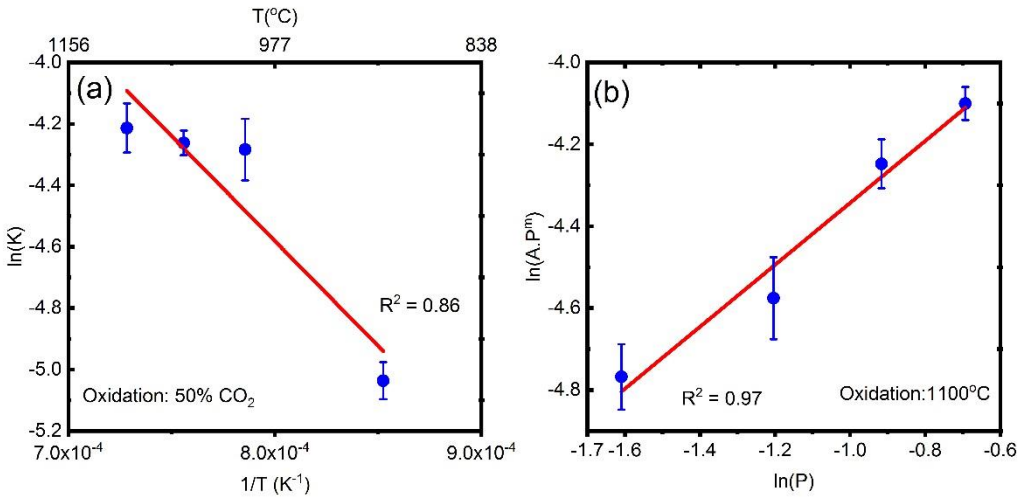

Figure 10 (a) ln(K) vs (1/T) Arrhenius plot of the oxidation reaction for AE3 model; (b) ln(AP^m) vs ln(P) plot for reduction reaction order determination

Similar validation studies were performed with the model fit and the experimental results. The values obtained match closely with the results presented by Farooqui et al [32] for oxidation of ceria following hydrogen reduction, where the activation energy obtained was 79 kJ/mol [32]. Nonetheless, curve fitting using the obtained value was performed and presented in the following Figure 11. Since the non-stoichiometry of reduction increases with the increase, it would be empirical to fix non-stoichiometry of a particular value to compare the reaction rate. Therefore reaction rate data of the model is compared with the experiments for those conditions in which δ_{red} reached 0.22. A good agreement of the results, both with respect to concentration and temperature variation can be seen. A slight over-estimation for lower concentrations are obtained like reduction, however, for higher concentrations a very good fit with is seen. An overall confidence level of the model with respect to experimental results of more than 95% is reached while agreeing well to the values obtained in similar studies performed reported in the literature.

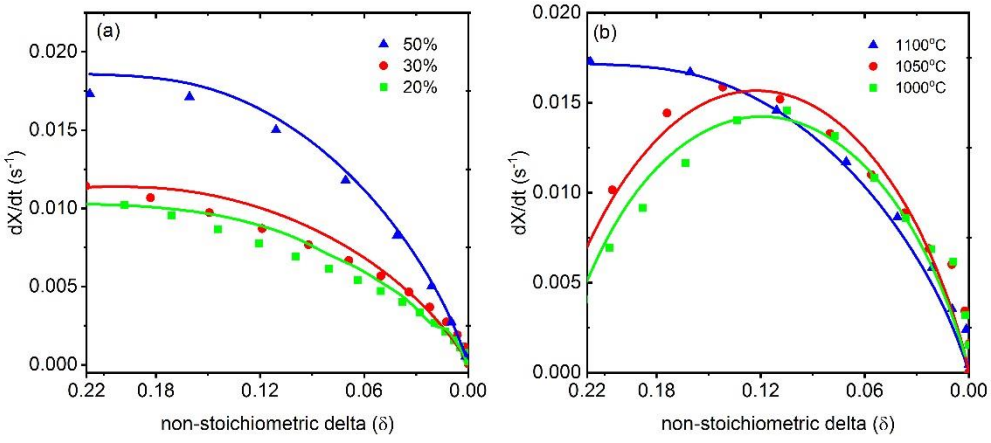

Figure 11 Comparison of the kinetic model and the experimental data for oxidation of reduced ceria with CO_2 (a) with the variation in concentration of CO_2 of 50%, 30% and 20% (b) with temperature of 1000°C, 1050°C, 1100°C for reactor pressure of 1 atm and a constant non-stoichiometric extent of reduced ceria of 0.22. The symbol represents experimental data and lines represent the kinetic model.

6. Effect of kinetics on the system analysis of an oxi-fired power plant

The oxyfuel power plant integrated with the chemical looping CO_2/H_2O splitting unit was investigated and presented in detail and the process flow diagram can be seen in Figure 12.

The power plant layout comprises of air separation unit (ASU) that feeds pure O_2 to the combustion chamber that is supplied by natural gas making it an oxyfuel power plant, therefore, a part of CO_2 captured from the exhaust is recirculated back to the combustion chamber to reduce the elevated temperature due to oxy-combustion and maintain outlet gas temperature inlet turbine temperature (TIT). As ASU consume huge power which renders a 13% efficiency penalty. A part of the exhaust gas mixture (CO_2/H_2O) is sent to the oxidation reactor of the CL unit. The oxidation reaction would yield additional syngas fuel which is sent to the combustion chamber for additional power production which would also lower the incoming natural gas requirement. As the exhaust gases from the gas turbines are at high temperatures leading the gases to have a steam ranking cycle with a heat recovery steam generator (HSRG). As the plant is oxy-combustion based there would be minimal SO_x and NO_x, therefore, the exhaust gases can be cooled down to ambient temperature. Apart from two streams, one to oxidation reactor another to the combustion chamber for recirculation, remaining CO_2 is sent for storage after a compression of 110 bar.

Main equipment of the proposed layout is chemical looping (CO_2/H_2O) unit (CL). Natural gas is fed to the combustion chamber of the power plant at a supply pressure of 70 bars that comes from network and expanded to CL unit operating pressure which is near atmospheric. The expanded natural gas is supplied to the reduction reactor (RED) where it undergoes partial oxidation of methane (POM) producing syngas. The operating conditions were selected to avoid complete oxidation or methane cracking. This reaction is endothermic and needs heat in order to maintain the continuous reaction. Ceria reduction by methane is reported to occur above 900^oC according to thermodynamics [55] studied we carried out and reported. Therefore, the RGIBBS reactor system of CL unit is replaced with moving bed reactors with reaction kinetics with the operating temperature at 1000^oC. Since a supplemental heat is required for reduction reactor an heat integration of combustion chamber of the power plant and reduction reactor is proposed with annular reactor design with inner reactor being reduction reactor of CL unit and annulus being combustion chamber providing excess heat [56]. More details of the system layout equipment operating conditions can be are reported in [55].

Hence, with the integration of CL unit, which recycles and converts a part of the exhaust gases to fuel, a net system efficiency improvement is expected for the conventional oxy-fired natural gas combined cycle with carbon capture of 100%.

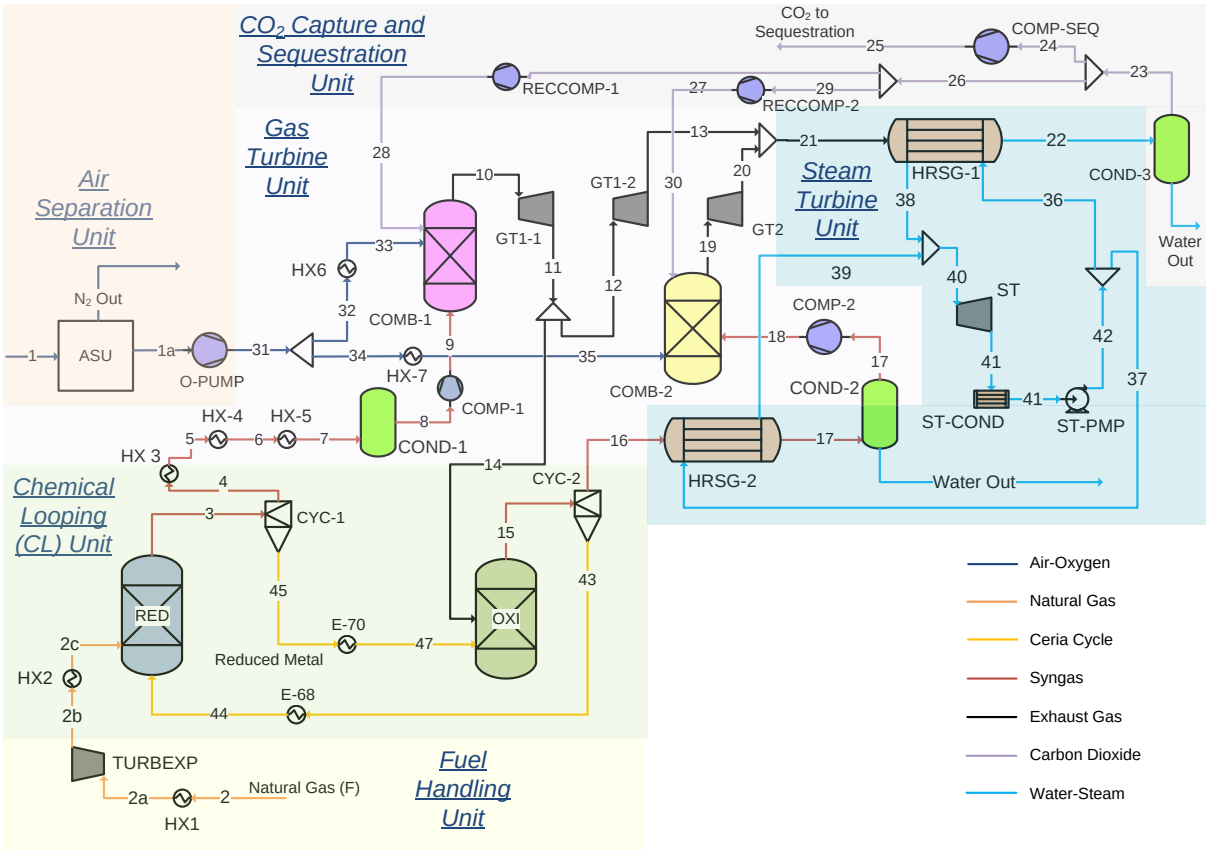

Figure 12. Process layout of oxi-fired power plant OXY-CC-CL[55]

6.1 Moving bed methane-driven chemical looping CO_2/H_2O splitting model

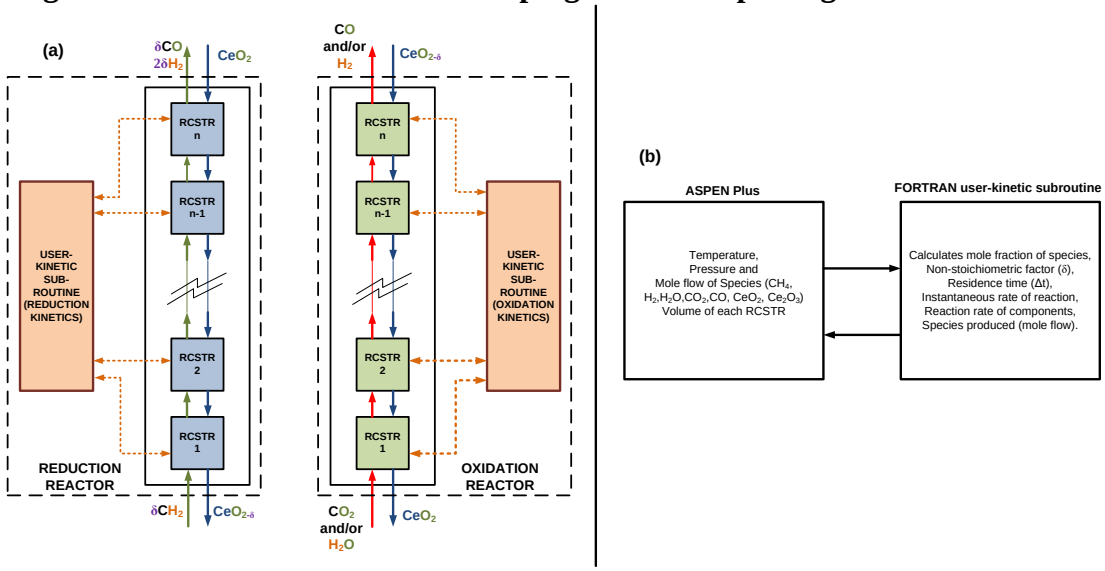

Figure 13 Moving bed reactor model for methane reduction and CO_2/H_2O oxidation reactors in ASPEN Plus hooked with user kinetics written in an external FORTRAN Code

Figure 13 represents the schematic of a counter-flow moving bed reactor system for reduction and oxidation reactor. In the reduction reactor (RED), ceria is introduced from the top by a hopper system (not shown) and it is reduced by incoming methane from the natural gas undergoing partial oxidation producing syngas ($CO+H_2$) flowing up to the top of the reactor in a counter-current with respect to ceria flow. In the oxidation reactor, reduced non-stoichiometric ceria is fed from the top and the exhaust gas from the turbine (CO_2+H_2O) is fed from the bottom which moves up reacting with the metal oxide undergoing splitting reaction producing CO and H_2. The oxidized ceria is transported away from the bottom by a rotating conveyor system (not shown) to the reduction reactor. Since the oxidation reaction is exothermic, there will be a ΔT along the length of the reactor.

Each reactor model is as a series of rigorously continuous stirred reactors (RCSTR) interconnected in Aspen Plus. The RCSTR reactor is widely used in the simulation for multiphase having characteristic of the same temperature for all phases. The total volume of the reactor is a summation of all the RCSTR reactors connected in series. The reaction kinetics developed by model fitting the experimental data is written in FORTRAN as a user-kinetic subroutine for both reduction and oxidation and hooked to each RCSTR reactor in the moving bed reactor model in Aspen plus shown in Figure 13. There are few specific assumptions were considered in developed reduction and oxidation reaction in moving bed reactors such as a) all the RCSTRs in reduction reactor is modelled as isothermal and for oxidation reactor as adiabatic reactors. The reduction and oxidation kinetic model developed considering all species taking part in reactions are described in the following section. The residence time in each RCSTRs was calculated based on the bed volume with respect to ceria in-flow neglecting the volume change due to change in the composition from reactions and lastly there is no change in the phase of ceria during redox recycling in the CL unit.

The number of RCSTRs selected for each reactor model relates to accuracy and time for simulation. Considering a methodology for optimizing the number of RCSTRs with respect to accuracy and the convergence time, an iterative procedure was adopted and relative change in the output of selectivity of CO and H2 at both the reactors were observed to be less than 0.25% which resulted in 10 RCSTRs for both reduction and oxidation reactor.

In Aspen plus, Broyden solver was selected with 500 iterations for both mass and energy solvers with a relative tolerance of 0.0001 and the PR-BM method which utilizes the Peng-Robinson cubic equation of state with the Bostone Mathias alpha function [57] is selected for the simulations.

6.2 Reduction and Oxidation kinetics

As previously reported in introduction the non-stoichiometric reaction (δ) of ceria during the methane reduction and oxidation steps follow the equations (3) and (2 and (22):

$$CeO_{2-\delta} + \delta H_2O \rightarrow CeO_2 + \delta H_2 \quad (22)$$

However, due to limited thermodynamic data available in the literature about the non-stoichiometric form of ceria ($CeO_{2-\delta}$), a different approach was adopted using the fully reduced form

of ceria Ce_2O_3, which is completely investigated in the literature. Consequently, the equations (3), (2) and (22) were rearranged in a different form (23-25):

$$CeO_2 + \delta CH_4 \rightarrow (1\text{-}2\cdot\delta)CeO_2 + \delta Ce_2O_3 + 2\cdot\delta H_2 + \delta CO \quad (23)$$

$$(1\text{-}2\cdot\delta)CeO_2 + \delta Ce_2O_3 + \delta CO_2 \rightarrow CeO_2 + \delta CO \quad (24)$$

$$(1\text{-}2\delta)CeO_2 + \delta Ce_2O_3 + \delta H_2O \rightarrow CeO_2 + \delta H_2 \quad (25)$$

In this case, the non-stoichiometric factor was used as an indicator of the ratio between the reduced ceria (Ce_2O_3) and the maximum amount of Ce_2O_3 achievable as described in equation (26).

$$\delta = \frac{\dot{n}_{Ce_2O_3}}{2\cdot\dot{n}_{Ce_2O_3} + \dot{n}_{CeO_2}} \quad (26)$$

Consequently, to a full reduced CeO_2 correspond a δ equal to 0.5. However, since the proposed kinetic is based on the non-stoichiometric reduction of ceria, in order to guarantee the stability of the lattice structure of the metal oxide, a limit to the δ equal to 0.35 (δ_{max}) was selected. Hence, according to the model proposed by Bulfin et al. [34], the degree of advancement of the reduction reaction, X_{RED}, was calculated as follow:

$$X_{RED} = \frac{\delta}{\delta_{max}} \quad (27)$$

So the reduction reaction is considered fully completed (X_{RED}=1) when the non-stoichiometric factor reaches the δ_{max}. While the degree of advancement of the oxidation reactor (X_{OXI}), which occurs in the opposite direction of reduction, was calculated as the complementary of X_{RED}.

$$X_{OXI} = 1\text{-}X_{RED} = 1\text{-}\frac{\delta}{\delta_{max}} \quad (28)$$

Correspondingly, a set of experiments were performed as explained section 4 and 5 to develop the same. The kinetic model assessment was determined to follow Avrami-Erofe'ev model (AE3) when ceria is reduced with methane. The model was tested for different concentrations and temperatures considering the reduction reaction (eq 3). From the reduction reaction, two moles of CeO_2 consumed to release one mole of Ce_2O_3 and one mole of CO and two moles of H_2.

Considering the reduction reaction (eq. 3) and the time-dependent equation for the degree of advancement of the reduction reaction that follows the AE3 kinetic model is given as equation (29).

$$\frac{dX_{RED}}{dx} = A_{RED}\cdot\exp\left(-\frac{E_{0,RED}}{RT}\right)\cdot 3(1\text{-}X_{RED})[-\ln(1\text{-}X_{RED})]^{2/3}\cdot[CH_4]^{m_{RED}} \quad (29)$$

$E_{0,RED}$ is the activation energy, A_{RED} is the pre-exponential constant with m_{RED} is the reactor order and their details are presented in section 5. The reaction rate constant for all the species involving in the reaction is represented by equation (30). The reaction coefficient (a_{RED}) for the three species taking part in the reaction are Table 1.

$$k_{RED\text{-}i} = a_{RED\text{-}i} \cdot \dot{n}_{CeO_2} \frac{dX_{RED}}{dt} \Delta t \tag{30}$$

$k_{RED\text{-}i}$ is rate constants of reduction species *i* listed as CeO_2, Ce_2O_3, CH_4, CO, H_2; Δt is the reaction time step which is calculated based on inlet volume flow of the ceria into the differential volume of the reactor and can be represented as:

$$\Delta t = \frac{\dot{V}_{OC,in}}{\Delta V_{reactor}} \tag{31}$$

Table 1 Reduction reaction coefficients

i	Reduction reaction coefficient (a_{RED})
CeO_2	-2
Ce_2O_3	1
CH_4	1
CO	1
H_2	2

Oxidation kinetics for CO_2 splitting also follow AE3 model as evaluated from the experimental analysis presented in section 5 is given by equation (32).

$$\frac{dX_{OXI\text{-}CO_2}}{dx} = A_{OXI\text{-}CO_2} \cdot \exp\left(-\frac{E_{0,OXI\text{-}CO_2}}{RT}\right) \cdot 3(1\text{-}X_{OXI\text{-}CO_2})[-\ln(1\text{-}X_{OXI\text{-}CO_2})]^{2/3} \cdot [CO_2]^{m_{RED}} \tag{32}$$

A_{OXI} and $E_{0,OXI}$ are the pre-exponential factor and the activation energy as presented in section 5. Methane reduction and consequently H_2O splitting reactivity was investigated earlier [46]. Since the CO_2 splitting reaction is the bottleneck oxidation reaction as it is slower and less exothermic compared to the H_2O splitting reaction, therefore the experimental investigation was done chosen CO_2 as an oxidizer.

For H_2O splitting, reaction kinetics model is adopted from Arifin [58] and Arifin and Weimer [59]. The reaction rate for oxidation reaction is represented as equation (33) and coefficients are presented in Table 3.

$$\frac{dX_{OXI\text{-}H_2O}}{dt} = A_{0,OXI\text{-}H_2O} \cdot \exp\left(-\frac{E_{0,OXI\text{-}H_2O}}{RT}\right) \cdot [H_2O]_i^{n_o} \cdot (1 - X_{OXI\text{-}H_2O})^{\psi_0} \tag{33}$$

$A_{0,OXI-H2O}$ is the Arrhenius constant, $E_{0,OXI-H2O}$ is the activation energy and n_o is the reaction order for the H_2O splitting reaction are listed in Table 2. The reaction rate constant for each species for the CO_2 and H_2O splitting is represented as equation (34 and 35).

Table 2 Kinetic parameters of the oxidation reaction of reduced ceria obtained by Arifin [59].

Oxidant	T (^oC)	$A_{0,OXI-H2O}$	$E_{0,OXI-H2O}$ (KJ/mol)	ψ_0 (-)	n_o(-)
H_2O	750-800	3.4	45	0.65	1.2
	825-875	2.5	41	0.7	1.7

$$k_{OXI-j} = a_{OXI-j} \cdot \dot{n}_{Ce_2O_3} \frac{dX_{OXI-j}}{dt} \Delta t \quad (34)$$

$$k_{OXI-l} = a_{OXI-l} \cdot \dot{n}_{Ce_2O_3} \left\{ \frac{dX_{OXI-H_2O}}{dt} + \frac{dX_{OXI-CO_2}}{dt} \right\} \Delta t \quad (35)$$

where k_{OXI-j} rates of oxidation species listed as H_2O, H_2, CO_2, CO and k_{OXI-l} is for CeO_2,Ce_2O_3 and the reaction coefficient (a_{OXI}) is given in Table 3.

Table 3 Oxidation reaction rate coefficient for water and carbon dioxide splitting.

j	Reaction coefficient (a_{OXI})	*l*	Reaction coefficient(a_{OXI})
H_2O	-1	CeO_2	2
H_2	1	Ce_2O_3	-1
CO_2	-1		
CO	1		

6.3 System performance

To improve on the thermodynamic evaluations reported by Farooqui et al [55], the RGIBBS reactors for the RED and OXI were replaced by moving bed reactors model, as developed in the previous section was integrated into the described OXY-CC-CL-K unit and the energetic performance of the proposed plant layout was evaluated. As for the oxidation reaction, since the primary component of the exhaust comprises over 86% CO_2, the available water splitting kinetics were used alongside the newly developed CO_2 splitting kinetics by in-house experiments described in the previous section 5. Based on the experimental results, an isothermal reduction reactor at 1000^oC was considered in the kinetic model. The heat integration and the annular combustion chamber concept was kept unchanged, whereby, the heat needed in the reduction reactor would be supplied from the heat generated in the combustion chamber. Additionally, the oxidation reactor was also considered a well-insulated adiabatic as opposed to a jacketed isothermal reactor at 1380^oC considered during the thermodynamic analysis.

To explain the comparative results of the overall plant performance, the need to understand separately, the efficiency of the CL unit as a separate entity and the efficiency of the entire layout is crucial. In this regard, the efficiency of the CL unit, calculated as per equation (36).

$$\eta_{SCL} = \frac{(\dot{m}_{H_2} LHV_{H_2} + \dot{m}_{CO} LHV_{CO})_{RED} + (\dot{m}_{H_2} LHV_{H_2} + \dot{m}_{CO} LHV_{CO})_{OXI}}{(\dot{m}_{CH_4} LHV_{CH_4} + (\dot{Q}_{RED} - \dot{Q}_{OXI}) + \dot{Q}_{NG}) + (\dot{Q}_{sphtr} - \dot{Q}_{sld})} \quad (36)$$

$\dot{Q}_{NG}$ is the heat necessary for heating the natural gas from after the turbo-expander to the condition necessary for the inlet to the reduction reactor; $\dot{Q}_{RED}$ is the heat requirement at the reduction reactor. Since the OXI is an adiabatic reactor, therefore, $\dot{Q}_{OXI}$ accounts for the net heat needed for the system operations, including the heat needed for heating inlet CO_2 and/or H_2O also the exothermic heat from splitting reactions. $\dot{Q}_{sld}$ represents the heat recovered from the solids from the reduction reactor before it enters oxidation, while $\dot{Q}_{spht}$ is the heat delivered to the solids for preheating. Since the exhaust of the turbine is directly sent to the oxidation unit, no heat-up of the same is necessary. Like before, the heat needed for heating of the solids and the heat required for cooling of the solids was not considered since an isothermal reactor system between the RED and the OXI was considered. However, it was ensured that no temperature cross-over takes place.

The results of the comparative evaluation of the performance of the CL unit from the thermodynamic to the kinetic evaluation is shown in Table 4. As can be seen, all other parameters being constant, the net energy rate content in the syngas formation in both the reactors is much less for the kinetic-based layout. Indeed, for a lower non-stoichiometry, more specifically 0.29 obtained in the reduction reactor of 10 m^3 volume, results in the production of a lower volume of syngas in both the reduction and oxidation reactor (with 6 m^3), unlike in thermodynamics, where a complete reduction of CeO_2 to Ce_2O_3 was assumed with an equivalent non-stoichiometry of 0.5. However, a lower non-stoichiometry also ensures the heating load of the reduction reactor to diminish, as compared to the thermodynamics levels. Nevertheless, the overall efficiency of the CL unit drops from 64.07% for ideal conditions to 42.88% for the evaluated operating conditions using developed reaction kinetic models. Also, it should be noted that the outlet temperature of the oxidized metal from the OXI drops to 1350^{o}C as opposed to 1380^{o}C obtained in the thermodynamic evaluation, requiring an additional heat removal of 4 MW. Nevertheless, such a high temperature of metal oxide in the RED, even though will considerably decrease the heat requirement of the reaction, might result in carbon deposition to occur as seen through experimental evaluations. Therefore, a detailed design optimization from multiple design perspectives needs to be assessed in further detail, which is beyond the scope of the present study.

Table 4 Comparison between the layout with thermodynamic and kinetic evaluation of the CL unit

Parameter	Units	OXY-CC-CL	OXY-CC-CL-K
The rate of Energy Content of Syngas from RED	MW	589.186	375.961
The rate of Energy Content of Syngas from OXI	MW	227.101	134.541
The rate of Net Energy in the Syngas Generated (H_2+CO)	MW	816.287	510.502
Q_{RED-IN}	MW	231.433	149.65
$Q_{OXY-OUT}$	MW	-4.44	0

Q_{NG}	MW	57.38	51.19
The rate of Energy Content in the Inlet Fuel (NG)	MW	989.667	989.667
η_{SCL}	-	64.07%	42.88%

However, unlike the efficiency of the CL unit, the plant efficiency depends not only on the net syngas generated in the CL unit but also on the total heat balance within the plant. Table 5 lists the comparison of the plant data for the thermodynamic assessment of the CL unit and the kinetic assessment of the same, all other parameters being kept constant. Since the combustion is a very highly exothermic and spontaneous reaction, no kinetic study is necessary to evaluate the reactions occurring in the combustion chamber, and no other chemical reactions occur in the entire plant. Indeed, interesting to note the net efficiency of the plant increases slightly from 50.7% for the thermodynamic model to 50.96% utilizing a kinetic model of the CL unit. Multiple points of comparison between the two analyses of the same layout can be observed.

The heat requirement in the reduction reactor decreases due to a lower reaction extent, resulting in a lower non-stoichiometry of the reduced ceria. In addition, based on the concept developed for the oxidation reactor for the solar reduction-based cycle, an excess of exhaust gas was sent to the reduction reactor increase the net power produced from syngas generation via splitting in the OXI. Additionally, being directly from the gas turbine outlet at a pressure of 2 bars, a high gas temperature of 921^{o}C at the inlet of the OXI was achieved. This results in the oxidized metal oxide temperature from the OXI to be at 1350^{o}C as opposed to 1380^{o}C for the thermodynamic layout.

Table 5 Plant Data Comparison of the layout based on thermodynamic (OXY-CC-CL) and kinetic evaluation of the CL unit (OXY-CC-CL-K)

Plant data	Units	OXY-CC-CL	OXY-CC-CL-K
Fuel Energy Input, LHV (A)	MW	990.708	990.708
Net GT Output	MW	484.233	523.488
ST Output	MW	255.937	251.003
Gross Electric Power Output (B)	MW	750.206	774.491
ASU Consumption + O_2 compression	MW	63.383	63.021
CO_2 Capture and Compression	MW	19.222	18.021
Power Cycle Pumps	MW	3.287	3.1
Air/ Recycled CO_2 Compression	MW	142.8797	153.61
Syngas Compressors	MW	17.1881	31.833
Total Parasitic Power Consumption (C)	MW	245.959	269.585
Net Electrical Power Output (D=B-C)	MW	504.247	504.906
Gross Electrical Efficiency (B/A*100)	MW	75.72%	78.18%
Net Electrical Efficiency (D/A*100)	%	50.70%	50.96%
CO_2 Capture Efficiency	%	100%	100%
CO_2 captured	t/h	178.658	178.658
Energy Output per tonne of CO_2 Captured	MWh/t	2.822	2.826

On the other hand, the gas outlet temperature from the OXI drops considerably. Due to a countercurrent reactor configuration, as well as from a lower reduction extent, the net exothermicity dropped considerably in the kinetic-based analysis than in the thermodynamic model based layout. Hence, the gas outlet temperature noted was 1120^{o}C, as opposed 1380^{o}C for the thermodynamic layout assessment. This lowers the heat availability within the system. However, the outlet temperature from the RED increases as well from 905^{o}C to 1000^{o}C from the thermodynamic to the kinetic model. Besides, the composition of the syngas produced being varying significantly between the two models; the heat transfer characteristics are different as well.

The heat requirement in the RED being significantly lower for the kinetic model (by 80 MW), while the TIT remains constant, the net CO_2 recycled for temperature control in the COMB increases. Thus, the power produced in the GT increases. However, this also increases, accordingly, the auxiliary power consumption in the CO_2 recycling compressor for COMB1. Nonetheless, both the energy production and consumption from auxiliary for the COMB2 cycle decreases due to a lower non-stoichiometry generated from reduction, as can be seen from the results in table 2. Furthermore, a lower temperature of the syngas from the OXI results in a lower steam generation in HRSG-2. Therefore, even though the gas expanded in GT1 and GT1-2 increases, the gas expanded in GT2 falls. The combined effect leads to a net drop in the power generated in the ST.

In summary, as can be followed from Table 5, the net efficiency of the power plant is governed by the output from the GT, by far the single largest energy generating unit of the power plant. Even though the auxiliary consumption increases, the net efficiency of the power plant increases slightly for a lower non-stoichiometry resulting from integrating kinetics of methane reduction and corresponding oxidation of the reduced metal oxide by CO_2 and H_2O. Nevertheless, it needs to be highlighted that similar to the thermodynamic system, the kinetic layout is also a non-optimized one. Therefore, to develop a more even comparison between the maximum achievable efficiency by complete heat integration between the two layouts, a pinch analysis for the latter is required as well.

A clear comparison to the pinch analysis of the layout using the thermodynamic assessment and kinetic-based layout, as presented in Figure 14 can be drawn. Unlike the available 350 MW of high-temperature heat above 200^{o}C for the thermodynamic layout, the system with the kinetics of the CL unit seems to be completely optimized without any heat available for further improvement of system performance. Therefore, the maximum achievable electrical efficiency is also limited to the present obtained value of 50.96%, as opposed to 61.5% achievable by system optimization of the thermodynamic layout. Nevertheless, even with kinetic limitations of the reduction and oxidation reactions, a reduction in the energy penalty, from 11.6 to only 3.8 percentage points is obtained, which would show the significant benefit of the proposed layout.

In fact, a net economic comparison with the thermodynamic layout was also performed, which are of interest due to the relative change in the sizes of the turbine and the compressors, resulting from a lower non-stoichiometry of ceria reduction. The total TOC of the plant was calculated as $1224 million, around $3 million lower than the corresponding CAPEX calculated using

thermodynamic evaluation of the layout. This change is however insignificant with respect to the other operating costs of the power plant as reported by Farooqui et al [55].

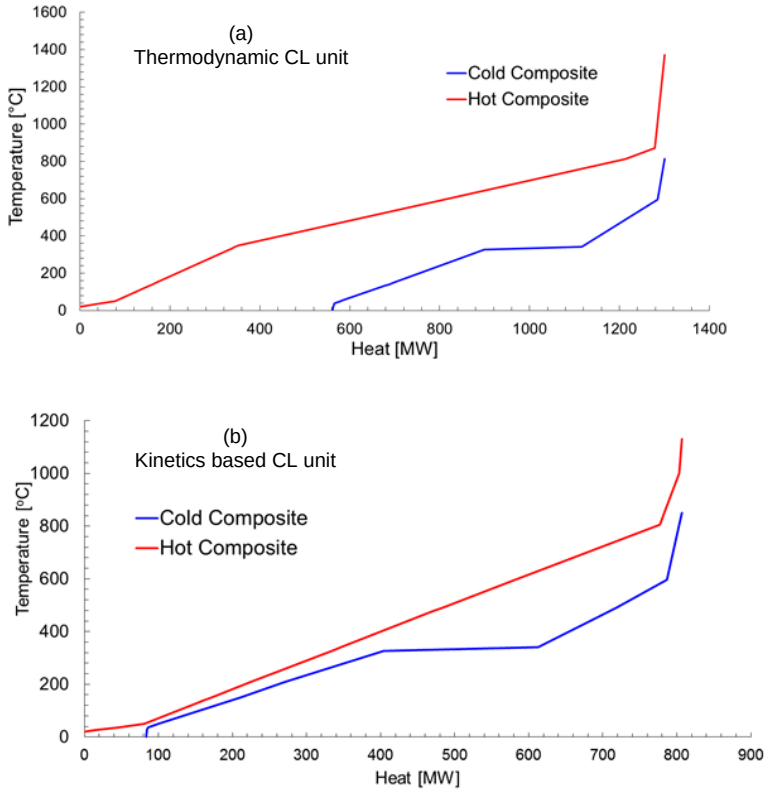

Figure 14 Pinch Analysis of the proposed plant based on (a) thermodynamics model OXY-CC-CL unit and (b) kinetics-based moving bed CL unit (OXY-CC-CL-K)

7. Conclusions

In the present study, we investigated the redox kinetics for commercial ceria considering methane for reduction that undergoes partial oxidation to syngas. For the oxidation step, CO_2 is used. The produced CO from both reduction and an oxidation step is evaluated for different temperatures (900-1100^oC) and methane concentrations (20-50%). It is observed that with an increase of temperature the CO production rate increases from 900-1050^oC and drops at 1000^oC. Even though at 1050^oC reveals to achieve higher CO production rate but the sample shows higher aggregates formation and carbon formation making it prone to deactivation of the sample. Similarly, for higher methane concentration, there is a drop in CO production rate which is also showed by SEM that there is carbon deposition. For oxidation, there is a relative increase in CO production with an increase in temperature but with minimal effect of CO_2 concentration. It is also observed that the reduction and oxidation kinetics paradigm has different reaction rates making methane reduction very slower compare to CO_2 splitting. Carbon deposition was noticed to small extents at 1050^oC, which increased subsequently at 1100^oC as evident from reactivity and microstructural studies. However, this can be followed from numerous discussions presented in the literature regarding the same.

Nevertheless, in the present study kinetic model fitting is carried out to describe the reaction of methane for syngas production with commercial ceria and corresponding oxidation with CO_2 over a wide range of temperature, 900-1100^oC, and concentration of the reactants. The entire reaction set-up was carried out in atmospheric conditions, indicating the high kinetic potential of the reduction reaction even at such conditions, as opposed to the thermal reduction of ceria, requiring deep vacuum conditions. The AE3 model was found to fit best to the experimental data for both the reduction and oxidation reactions. A varying reaction order with varying reaction conditions was noticed and a relation was obtained for both the cases. Carbon deposition would limit the operation of the reduction at temperatures over 1100^oC, even though a very fast reaction would result.

Application of the derived kinetics was used to investigate the effect of kinetics based reactors on the system performance that considering chemical looping CO_2/H_2O splitting in reduction and oxidation reactors. A moving bed reactors system is developed considered number of RCSTRs in series in Aspen Plus to mimic the moving bed behavior of gas and solid in counter-flow direction with kinetics hooked using a user-kinetic subroutine. The developed CL unit is integrated with an oxy-fueled power natural gas combined cycle power plant and effect of kinetics on chemical looping unit performance and overall system layout performance is evaluated. With kinetics, the maximum reaction extent relates as non-stoichiometry of ceria reached was 0.29 and the CL unit efficiency (η_{SCL}) was found to be 42.8% compared to 64% when thermodynamics is considered in CL unit. Similarly, the electrical efficiency of the whole plant was 50.9% with kinetics instead of 61% when thermodynamics is considered. A pinch point analysis is also performed in order to investigate if their system is tightly integrated for heat balance. Therefore, from the above analysis, it can be concluded that there is a significant effect of kinetics and the reactor system for chemical looping CO_2/H_2O dissociation integration to the power plants. The above analysis is a significant step in retrofitting existing natural gas-fired power plants with the possibility of extending it to other fossil fuel power plants.

References

[1] D.Y.C. Leung, G. Caramanna, M.M. Maroto-Valer, An overview of current status of carbon dioxide capture and storage technologies, Renew. Sustain. Energy Rev. 39 (2014) 426–443. doi:10.1016/j.rser.2014.07.093.

[2] Y.A. Daza, R.A. Kent, M.M. Yung, J.N. Kuhn, Carbon dioxide conversion by reverse water-gas shift chemical looping on perovskite-type oxides, Ind. Eng. Chem. Res. 53 (2014) 5828–5837. doi:10.1021/ie5002185.

[3] J. Kim, C.A. Henao, T.A. Johnson, D.E. Dedrick, J.E. Miller, E.B. Stechel, C.T. Maravelias, Methanol production from CO2 using solar-thermal energy: process development and techno-economic analysis, Energy Environ. Sci. 4 (2011) 3122. doi:10.1039/c1ee01311d.

[4] S. Abanades, H.I. Villafan-Vidales, CO2 and H2O conversion to solar fuels via two-step solar

thermochemical looping using iron oxide redox pair, Chem. Eng. J. 175 (2011) 368–375. doi:10.1016/j.cej.2011.09.124.

[5] S. Abanades, G. Flamant, Thermochemical hydrogen production from a two-step solar-driven water-splitting cycle based on cerium oxides, Sol. Energy. 80 (2006) 1611–1623. doi:10.1016/j.solener.2005.12.005.

[6] W.C. Chueh, C. Falter, M. Abbott, D. Scipio, P. Furler, S.M. Haile, A. Steinfeld, High-Flux Solar-Driven Thermochemical Dissociation of CO2 and H2O Using Nonstoichiometric Ceria, Science (80-.). 330 (2010) 1797–1801. doi:10.1126/science.1197834.

[7] P. Furler, J. Scheffe, M. Gorbar, L. Moes, U. Vogt, A. Steinfeld, Solar Thermochemical CO 2 Splitting Utilizing a Reticulated Porous Ceria Redox System, Energy & Fuels. 26 (2012) 7051–7059. doi:10.1021/ef3013757.

[8] P. Furler, J.R. Scheffe, A. Steinfeld, Syngas production by simultaneous splitting of H2O and CO 2 via ceria redox reactions in a high-temperature solar reactor, Energy Environ. Sci. 5 (2012) 6098–6103. doi:10.1039/C1EE02620H.

[9] K. Otsuka, Y. Wang, E. Sunada, I. Yamanaka, Direct partial oxidation of methane to synthesis gas by cerium oxide, J. Catal. 175 (1998) 152–160. doi:10.1006/jcat.1998.1985.

[10] Y. Kiyoshi, Otsuka; Tetsuya, Ushiyama; Ichiro, Partial oxidation of methane using the redox of cerium oxide, Chem. Lett. (1993) 1517–1520.

[11] D. Arifin, A.W. Weimer, Kinetics and mechanism of solar-thermochemical H2 and CO production by oxidation of reduced CeO2, Sol. Energy. 160 (2018) 178–185. doi:10.1016/j.solener.2017.11.075.

[12] P.T. Krenzke, J.R. Fosheim, J.H. Davidson, Solar fuels via chemical-looping reforming, Sol. Energy. 156 (2017) 48–72. doi:10.1016/j.solener.2017.05.095.

[13] K.J. Warren, J. Reim, K. Randhir, B. Greek, R. Carrillo, D.W. Hahn, J.R. Scheffe, Theoretical and Experimental Investigation of Solar Methane Reforming through the Nonstoichiometric Ceria Redox Cycle, Energy Technol. 5 (2017) 2138–2149. doi:10.1002/ente.201700083.

[14] C.K. Yang, Y. Yamazaki, A. Aydin, S.M. Haile, J.R. Scheffe, J. Li, A.W. Weimer, K. Otsuka, M. Hatano, A. Morikawa, E.S. Material, M.C.A. This, T.R. Society, M. Kang, X. Wu, J. Zhang, N. Zhao, W. Wei, Y. Sun, J.R. Scheffe, R. Jacot, G.R. Patzke, A. Steinfeld, A. Le Gal,

S. Abanades, Y. Hao, C.K. Yang, S.M. Haile, M.E. Gálvez, R. Jacot, J.R. Scheffe, T. Cooper, G.R. Patzke, A. Steinfeld, I. Ermanoski, J.E. Miller, M.D. Allendorf, S. Dey, B.S. Naidu, C.N.R.R. Rao, A. Govindaraj, C.N.R.R. Rao, A. Demont, S. Abanades, T.C. Davenport, M. Kemei, M.J. Ignatowich, S.M. Haile, P. Singh, M.S. Hegde, S. Dey, B.S. Naidu, A. Govindaraj, C.N.R.R. Rao, L. Zhu, Y. Lu, W.C. Chueh, M. Abbott, D. Scipio, S.M. Haile, A. Le Gal, S. Abanades, R. Fernández-Saavedra, M.B. Gómez-Mancebo, C. Caravaca, M. Sánchez, A.J. Quejido, A. Vidal, F. Fresno, R. Fernández-Saavedra, M. Belén Gómez-Mancebo, A. Vidal, M. Sánchez, M. Isabel Rucandio, A.J. Quejido, M. Romero, T.C. Davenport, M. Kemei, M.J. Ignatowich, S.M. Haile, L. Nalbandian, A. Evdou, V. Zaspalis, A. Steinfeld, V.M. Wheeler, R. Bader, P.B. Kreider, M. Hangi, S. Haussener, W. Lipiński, T. Kodama, S. Bellan, N. Gokon, H.S. Cho, C.P. Falter, A. Sizmann, R. Pitz-Paal, C. Jarrett, W.C. Chueh, C. Yuan, Y. Kawajiri, K.H. Sandhage, A. Henry, N. Gokon, H. Murayama, A. Nagasaki, T. Kodama, I. Alxneit, T. Kodama, Y. Kondoh, R. Yamamoto, H. Andou, N. Satou, H. Kaneko, T. Kodama, N. Gokon, Y. Tamaura, K. Lovegrove, A. Luzzi, K. Ehrensberger, A. Frei, P. Kuhn, H.R. Oswald, P. Hug, D. Arifin, A.W. Weimer, S. Abanades, G. Flamant, A. Le Gal, S. Abanades, G. Flamant, Q. Jiang, G. Zhou, Z. Jiang, C. Li, C. Agrafiotis, M. Roeb, C. Sattler, W.C. Chueh, S.M. Haile, N. Gokon, S. Sagawa, T. Kodama, Q. Jiang, J. Tong, G. Zhou, Z. Jiang, Z. Li, C. Li, A. Le Gal, S. Abanades, P. Furler, J.R. Scheffe, A. Steinfeld, R. Bala Chandran, J.H. Davidson, E.N. Coker, J.A. Ohlhausen, A. Ambrosini, J.E. Miller, A.H. McDaniel, A. Ambrosini, E.N. Coker, J.E. Miller, W.C. Chueh, R. O'Hayre, J. Tong, T. Nakamura, S. Abanades, Interplay of material thermodynamics and surface reaction rate on the kinetics of thermochemical hydrogen production, Sol. Energy. 17 (2015) 16932–16945. doi:10.1016/j.ijhydene.2017.05.184.

[15] F. Lin, M. Rothensteiner, I. Alxneit, J.A. van Bokhoven, A. Wokaun, First demonstration of direct hydrocarbon fuel production from water and carbon dioxide by solar-driven thermochemical cycles using rhodium–ceria, Energy Environ. Sci. (2016). doi:10.1039/C6EE00862C.

[16] F. Lin, A. Wokaun, I. Alxneit, Rh-doped Ceria: Solar Organics from H2O, CO2 and Sunlight?, in: Energy Procedia, 2015. doi:10.1016/j.egypro.2015.03.151.

[17] M.M. Nair, S. Abanades, Tailoring Hybrid Nonstoichiometric Ceria Redox Cycle for Combined Solar Methane Reforming and Thermochemical Conversion of H2O/CO2, Energy and Fuels. 30 (2016) 6050–6058. doi:10.1021/acs.energyfuels.6b01063.

[18] T. Kodama, N. Gokon, Thermochemical cycles for high-temperature solar hydrogen production, Chem. Rev. 107 (2007) 4048–4077. doi:10.1021/cr050188a.

[19] S. Lorentzou, D. Dimitrakis, A. Zygogianni, G. Karagiannakis, A.G. Konstandopoulos, Thermochemical H2O and CO2splitting redox cycles in a NiFe2O4structured redox reactor: Design, development and experiments in a high flux solar simulator, Sol. Energy. 155 (2017) 1462–1481. doi:10.1016/j.solener.2017.07.001.

[20] J. Lapp, Thermal modeling and design of a solar non-stoichiometric redox reactor with heat recovery, (2013). http://conservancy.umn.edu/handle/11299/159856.

[21] M. Roeb, C. Sattler, R. Klüser, N. Monnerie, L. de Oliveira, A.G. Konstandopoulos, C. Agrafiotis, V.T. Zaspalis, L. Nalbandian, A. Steele, P. Stobbe, Solar Hydrogen Production by a Two-Step Cycle Based on Mixed Iron Oxides, J. Sol. Energy Eng. 128 (2006) 125. doi:10.1115/1.2183804.

[22] T.C. Davenport, C.K. Yang, C.J. Kucharczyk, M.J. Ignatowich, S.M. Haile, Maximizing fuel production rates in isothermal solar thermochemical fuel production, Appl. Energy. 183 (2016) 1098–1111. doi:10.1016/j.apenergy.2016.09.012.

[23] M. Welte, K. Warren, J.R. Scheffe, A. Steinfeld, Combined Ceria Reduction and Methane Reforming in a Solar-Driven Particle-Transport Reactor, Ind. Eng. Chem. Res. 56 (2017). doi:10.1021/acs.iecr.7b02738.

[24] K.J. Warren, J. Reim, K. Randhir, B. Greek, R. Carrillo, D.W. Hahn, J.R. Scheffe, Theoretical and Experimental Investigation of Solar Methane Reforming through the Nonstoichiometric Ceria Redox Cycle, Energy Technol. 5 (2017) 2138–2149. doi:10.1002/ente.201700083.

[25] K. Otsuka, T. Ushiyama, I. Yamanaka, Partial Oxidation of Methane Using the Redox of Cerium Oxide, Chem. Lett. 22 (1993) 1517–1520. doi:10.1246/cl.1993.1517.

[26] K. Otsuka, E. Sunada, T. Ushiyama, I. Yamanaka, The production of synthesis gas by the redox of cerium oxide, in: M. de Pontes, R.L. Espinoza, C.P. Nicolaides, J.H. Scholtz, M.S.B.T.-S. in S.S. and C. Scurrell (Eds.), Nat. Gas Convers. IV, Elsevier, 1997: pp. 531–536. doi:https://doi.org/10.1016/S0167-2991(97)80386-2.

[27] K.J. Warren, J.R. Scheffe, Kinetic insights into the reduction of ceria facilitated via the partial oxidation of methane, Mater. Today Energy. 9 (2018) 39–48. doi:10.1016/j.mtener.2018.05.001.

[28] T. Ishida, N. Gokon, T. Hatamachi, T. Kodama, Kinetics of thermal reduction step of thermochemical two-step water splitting using CeO2 particles: Master-plot method for analyzing non-isothermal experiments, Energy Procedia. 49 (2013) 1970–1979. doi:10.1016/j.egypro.2014.03.209.

[29] A. Le Gal, S. Abanades, Catalytic investigation of ceria-zirconia solid solutions for solar hydrogen production, Int. J. Hydrogen Energy. 36 (2011) 4739–4748. doi:10.1016/j.ijhydene.2011.01.078.

[30] F.J. Gotor, José, M. Criado, J. Malek, N. Koga, Kinetic analysis of solid-state reactions: The universality of master plots for analyzing isothermal and nonisothermal experiments, J. Phys. Chem. A. 104 (2000) 10777–10782. doi:10.1021/jp0022205.

[31] A. Khawam, D.R. Flanagan, Solid-State Kinetic Models: Basics and Mathematical Fundamentals, J. Phys. Chem. B. 110 (2006) 17315–17328. doi:10.1021/jp062746a.

[32] A.E. Farooqui, A.M. Pica, P. Marocco, D. Ferrero, A. Lanzini, S. Fiorilli, J. Llorca, M. Santarelli, Assessment of kinetic model for ceria oxidation for chemical-looping CO2 dissociation, Chem. Eng. J. 346 (2018) 171–181. doi:10.1016/j.cej.2018.04.041.

[33] J.R. Scheffe, A.H. McDaniel, M.D. Allendorf, A.W. Weimer, Kinetics and mechanism of solar-thermochemical H2 production by oxidation of a cobalt ferrite–zirconia composite, Energy Environ. Sci. 6 (2013) 963. doi:10.1039/c3ee23568h.

[34] B. Bulfin, A.J. Lowe, K.A. Keogh, B.E. Murphy, O. Lübben, S.A. Krasnikov, I. V. Shvets, Analytical Model of CeO 2 Oxidation and Reduction, J. Phys. Chem. C. 117 (2013) 24129–24137. doi:10.1021/jp406578z.

[35] J. Kim, T.A. Johnson, J.E. Miller, E.B. Stechel, C.T. Maravelias, Fuel production from CO2 using solar-thermal energy: system level analysis, Energy Environ. Sci. 5 (2012) 8417. doi:10.1039/c2ee21798h.

[36] C. Falter, V. Batteiger, A. Sizmann, Climate Impact and Economic Feasibility of Solar Thermochemical Jet Fuel Production, Environ. Sci. Technol. 50 (2016) 470–477. doi:10.1021/acs.est.5b03515.

[37] C. Falter, R. Pitz-Paal, Energy analysis of solar thermochemical fuel production pathway with a focus on waste heat recuperation and vacuum generation, Sol. Energy. 176 (2018) 230–240. doi:10.1016/J.SOLENER.2018.10.042.

[38] L. Zhu, Y. Lu, Reactivity and efficiency of ceria-based oxides for solar CO2 splitting via isothermal and near-isothermal cycles, Energy & Fuels. (2017) acs.energyfuels.7b03284. doi:10.1021/acs.energyfuels.7b03284.

[39] C. Muhich, A. Steinfeld, Principles of doping ceria for the solar thermochemical redox splitting of H $_2$O and CO $_2$, J. Mater. Chem. A. 5 (2017) 15578–15590. doi:10.1039/C7TA04000H.

[40] S. Ackermann, L. Sauvin, R. Castiglioni, J.L.M. Rupp, J.R. Scheffe, A. Steinfeld, Kinetics of CO2 Reduction over Nonstoichiometric Ceria, J. Phys. Chem. C. 119 (2015) 16452–16461. doi:10.1021/acs.jpcc.5b03464.

[41] L.J. Venstrom, R.M. De Smith, Y. Hao, S.M. Haile, J.H. Davidson, Efficient Splitting of CO 2 in an Isothermal Redox Cycle Based on Ceria, Energy & Fuels. 28 (2014) 2732–2742. doi:10.1021/ef402492e.

[42] Z. Zhao, M. Uddi, N. Tsvetkov, B. Yildiz, A.F. Ghoniem, Redox Kinetics Study of Fuel Reduced Ceria for Chemical-Looping Water Splitting, J. Phys. Chem. C. 120 (2016) 16271–16289. doi:10.1021/acs.jpcc.6b01847.

[43] S.G. Rudisill, L.J. Venstrom, N.D. Petkovich, T. Quan, N. Hein, D.B. Boman, J.H. Davidson, A. Stein, Enhanced Oxidation Kinetics in Thermochemical Cycling of CeO 2 through Templated Porosity, J. Phys. Chem. C. 117 (2013) 1692–1700. doi:10.1021/jp309247c.

[44] S. Chuayboon, S. Abanades, S. Rodat, Syngas production via solar-driven chemical looping methane reforming from redox cycling of ceria porous foam in a volumetric solar reactor, Chem. Eng. J. 356 (2018) 756–770. doi:10.1016/j.cej.2018.09.072.

[45] W.C. Chueh, M. Abbott, D. Scipio, S.M. Haile, High-flux solar-driven thermochemical dissociation of CO 2 and H 2 O using ceria redox reactions, Science (80-.). 63 (2010) 2010. doi:10.1123/science.1197834.

[46] Z. Zhao, Redox kinetics study for chemical looping combustion, water and CO2 splitting using nickel and cerium based oxygen carrier, Massachusetts institute of technology, 2016.

[47] B. Janković, B. Adnađević, S. Mentus, The kinetic study of temperature-programmed reduction of nickel oxide in hydrogen atmosphere, Chem. Eng. Sci. 63 (2008) 567–575. doi:10.1016/j.ces.2007.09.043.

[48] L. Han, Z. Zhou, G.M. Bollas, Heterogeneous modeling of chemical-looping combustion. Part 1: Reactor model, Chem. Eng. Sci. 104 (2013) 233–249. doi:10.1016/j.ces.2013.09.021.

[49] Z. Zhao, M. Uddi, N. Tsvetkov, B. Yildiz, A.F. Ghoniem, Enhanced intermediate-temperature CO 2 splitting using nonstoichiometric ceria and ceria–zirconia, Phys. Chem. Chem. Phys. 19 (2017) 25774–25785. doi:10.1039/C7CP04789D.

[50] Galwey AK; Brown ME, Kinetic background to thermal analysis and calorimetry, in: Handb. Therm. Anal. Calorim. Vol. 1 Princ. Pract., 1998: pp. 147–216.

[51] S. Ackermann, J.R. Scheffe, A. Steinfeld, Diffusion of oxygen in ceria at elevated temperatures and its application to H2O/CO2 splitting thermochemical redox cycles, J. Phys. Chem. C. 118 (2014) 5216–5225. doi:10.1021/jp500755t.

[52] P. Pantu, K. Kim, G.R. Gavalas, Methane partial oxidation on Pt/CeO2–ZrO2 in the absence of gaseous oxygen, Appl. Catal. A Gen. 193 (2000) 203–214. doi:10.1016/S0926-860X(99)00429-9.

[53] A. Steinfeld, A. Frei, P. Kuhn, D. Wuillemin, Solar thermal production of zinc and syngas via combined ZnO-reduction and CH4-reforming processes, Int. J. Hydrogen Energy. 20 (1995) 793–804. doi:10.1016/0360-3199(95)00016-7.

[54] X. Zhu, H. Wang, Y. Wei, K. Li, X. Cheng, Hydrogen and syngas production from two-step steam reforming of methane using CeO2as oxygen carrier, J. Nat. Gas Chem. 20 (2011) 281–286. doi:10.1016/S1003-9953(10)60185-5.

[55] A. Farooqui, A. Bose, D. Ferrero, J. Llorca, M. Santarelli, Techno-economic and exergetic assessment of an oxy-fuel power plant fueled by syngas produced by chemical looping CO2 and H2O dissociation, J. CO2 Util. 27 (2018) 500–517. doi:10.1016/j.jcou.2018.09.001.

[56] M.N. Khan, T. Shamim, Influence of Specularity Coefficient on the Hydrodynamics and Bubble Statistics of an Annular Fluidized Bed Reactor, Energy Procedia. 105 (2017) 1998–2003. doi:10.1016/j.egypro.2017.03.573.

[57] J. Fan, L. Zhu, P. Jiang, L. Li, H. Liu, Comparative exergy analysis of chemical looping combustion thermally coupled and conventional steam methane reforming for hydrogen production, J. Clean. Prod. 131 (2016) 247–258. doi:10.1016/j.jclepro.2016.05.040.

[58] D. Arifin, Study of redox reactions to split water and carbon dioxide, University of Colorado,

2013. http://scholar.colorado.edu/chbe_gradetds/54.

[59] D. Arifin, A.W. Weimer, Kinetics and mechanism of solar-thermochemical H2and CO production by oxidation of reduced CeO2, Sol. Energy. 160 (2018) 178–185. doi:10.1016/j.solener.2017.11.075.